

JPRS-UMS-92-010
30 JUNE 1992



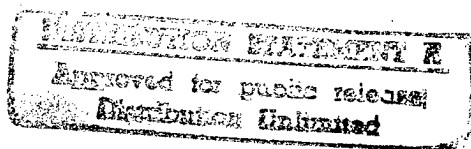
**FOREIGN
BROADCAST
INFORMATION
SERVICE**

JPRS Report

Science & Technology

***Central Eurasia:
Materials Science***

19980116 192



DTIC QUALITY INSPECTED 2

REPRODUCED BY
U.S. DEPARTMENT OF COMMERCE
NATIONAL TECHNICAL INFORMATION SERVICE
SPRINGFIELD, VA. 22161

Science & Technology

Central Eurasia: Materials Science

JPRS-UMS-92-010

CONTENTS

30 June 1992

Analysis, Testing

Electron Emission From Metals Bombarded by Fast Multiple-Charge Ions [V.V. Katin, Yu.V. Martynenko, et al.; <i>POVERKHNOST: FIZIKA, KHIMIYA, MEKHANIKA</i> , No 1, Jan 92]	1
Enthalpy of the Formation of Melts of the System Cr-Si-C [V.T. Vitusevich; <i>ROSSIYSKAYA AKADEMIYA NAUK: SERIYA METALLY</i> , No 1, Jan-Feb 92]	1
Oxide Formation in Chromium Condensates at Elevated Temperatures [M.V. Belous, L.P. Germash, et al.; <i>ROSSIYSKAYA AKADEMIYA NAUK: SERIYA METALLY</i> , No 1, Jan-Feb 92]	2
New Phenomenon in Solid Material Under Compression to Ultrahigh Pressure [V.A. Shapochkin, Ye.V. Shapochkina; <i>FIZIKA I KHIMIYA OBRABOTKI MATERIALOV</i> , No 1, Jan-Feb 92]	2
Fracture Analysis of Cast Steel and Pig Iron From Synergetic Viewpoint [I.P. Volchok, O.B. Kolotilkin; <i>ROSSIYSKAYA AKADEMIYA NAUK: SERIYA METALLY</i> , No 2, Mar-Apr 92]	2
Laser Probing of Initial Stage of $\gamma \rightarrow \alpha$ Martensite Transformation [M.P. Kashchenko, V.V. Letuchev, et al.; <i>ROSSIYSKAYA AKADEMIYA NAUK: SERIYA METALLY</i> , No 2, Mar-Apr 92]	3
Change in Hydrogen Solubility in Metals at Melting Point [V.I. Lakomskiy; <i>ROSSIYSKAYA AKADEMIYA NAUK: SERIYA METALLY</i> , No 2, Mar-Apr 92]	3
Thermodynamic Properties of Fe-Ni-O and Fe-Ni-O-Ta-Si System Melts [V.S. Sudavitsova, N.O. Sharkina; <i>ROSSIYSKAYA AKADEMIYA NAUK: SERIYA METALLY</i> , No 2, Mar-Apr 92]	3
Role of Plastic Deformation in Structure Formation of Ceramic Materials [G.S. Oleynik; <i>POROSHKOVAYA METALLURGIYA</i> , No 3 (351), Mar 92]	4
Resistance of Titanium Carbide Powders Synthesized by Various Methods to H_2O_2 and H_2SO_4 Solutions [G.N. Komratov, I.D. Chausskaya; <i>POROSHKOVAYA METALLURGIYA</i> , No 3 (351), Mar 92]	4
On Problem of Lowering Light Absorption by Films in Infrared Spectrum [Ye.N. Kotlov, D.N. Gromov, et al.; <i>VYSOKOCHISTYYE VESHCHESTVA</i> , No 2, Mar-Apr 92]	4
Tandem Laser-Probe Mass-Reflectron [I.D. Kovalev, P.A. Shmonin; <i>VYSOKOCHISTYYE VESHCHESTVA</i> , No 2, Mar-Apr 92]	4

Coatings

Porosity and Protective Action of Aluminum Galvanic Coatings [V. V. Krasnoyarskiy, V. A. Mazin, et al.; <i>Moscow ZASHCHITA METALLOV</i> , Vol 28 No 1, Jan-Feb 92]	6
Role of Hydrogen in the Formation of Silky Mat Coatings [S.S. Kruglikov, N.G. Bakhchisaraytsyan, et al.; <i>ZASHCHITA METALLOV</i> , Vol 28 No 2, Mar-Apr 92]	6
Laser-Stimulated Electrodeposition of a Tin-Bismuth Alloy [Yu.V. Seryanov, L.V. Aravina; <i>ZASHCHITA METALLOV</i> , Vol 28 No 2, Mar-Apr 92]	6
Effect of Organic Surfactants on the Composition of Galvanic Alloys [Yu.P. Perelygin; <i>ZASHCHITA METALLOV</i> , Vol 28 No 2, Mar-Apr 92]	7
Composition of Cu-Ni Films Deposited on Substrate While Sputtered by Ar Ions [K.V. Kosterin; <i>FIZIKA I KHIMIYA OBRABOTKI MATERIALOV</i> , No 1, Jan-Feb 92]	7
On Mechanism of Chromium-Based Diffusion Coat Formation on Steel [V.N. Mikhaylin, B.N. Chertov, et al.; <i>ROSSIYSKAYA AKADEMIYA NAUK: SERIYA METALLY</i> , No 2, Mar-Apr 92]	7
Gallium Interaction With Aluminum Films [G.F. Ivin; <i>ROSSIYSKAYA AKADEMIYA NAUK: SERIYA METALLY</i> , No 2, Mar-Apr 92]	8

Plasma Coats From Zirconium Dioxide Powder Produced by Sol-Gel Technology [I.N. Gorbatoev, A.Ye. Terentyev, et al.; POROSHKOVAYA METALLURGIYA, No 3 (351), Mar 92]	8
Aluminum Oxide Electric Insulation Plasma Coats for Radio Electronic Equipment Heat Sinks [V.G. Zilberberg, A.M. Vyaltsev, et al.; POROSHKOVAYA METALLURGIYA, No 3 (351), Mar 92]	8

Corrosion

Conjugate Processes During the Electrolytic Dissolution of Metals and Alloys [V. Yu. Kondrashin; Moscow ZASHCHITA METALLOV, Vol 28 No 1, Jan-Feb 92]	9
Estimating the Stationary Corrosion Rate of Metals Under Atmospheric Conditions [Din Vu; Moscow ZASHCHITA METALLOV, Vol 28 No 1, Jan-Feb 92]	9
Corrosion Behavior of Sintered Heterophase TiN-Cr and TiN-Ni Materials in Sulfuric Acid Solution [T. V. Chukalovskaya, N. D. Tomashov, et al.; Moscow ZASHCHITA METALLOV, Vol 28 No 1, Jan-Feb 92]	9
Corrosion Behavior of Chromized Steel 45 in Sulfuric and Hydrochloric Acid Solutions [S. G. Babich, V. M. Knyazheva, et al.; Moscow ZASHCHITA METALLOV, Vol 28 No 1, Jan-Feb 92]	9
Corrosion of Ferrous Metals in Solutions of Zinc Bromide and Calcium Bromide [V. N. Gnusin, V. A. Mosin, et al.; Moscow ZASHCHITA METALLOV, Vol 28 No 1, Jan-Feb 92]	10
Effect of Pre-Carburization on the Anti-Corrosion Properties of Chromized Low-Carbon Steel [I. S. Litmanovich, Ya. M. Zolotovitskiy; Moscow ZASHCHITA METALLOV, Vol 28 No 1, Jan-Feb 92]	10
Corrosion of Steel and Nickel Steel Alloys in Nitrosylchloride [B. A. Gru, A. I. Tsinman, et al.; Moscow ZASHCHITA METALLOV, Vol 28 No 1, Jan-Feb 92]	10
The Electrochemical and Corrosion Behavior of Nickel in Sulfuric Acid Solutions [A.E. Kozachinskiy, A.P. Pchel'nikov, et al.; ZASHCHITA METALLOV, Vol 28 No 2, Mar-Apr 92]	11
The Corrosion and Electrochemical Behavior of Aluminum-Iron-Nickel Bronze in a Chloride Solution [V.N. Chervyakov, L.V. Kharkova, et al.; ZASHCHITA METALLOV, Vol 28 No 2, Mar-Apr 92]	11
The Impedance of a Corroding Titanium Electrode in Acid Solutions [Kh.G. Kuchukbayev, V.I. Kichigin, et al.; ZASHCHITA METALLOV, Vol 28 No 2, Mar-Apr 92]	11
The Effect of Lithium Additives on the Corrosion Properties of Aluminum [V.S. Sinyavskiy, A.M. Semenov, et al.; ZASHCHITA METALLOV, Vol 28 No 2, Mar-Apr 92]	12
The Effect of Diamond Smoothing on the Resistance of Cr17Ni15 Steel to Chloride Corrosion Cracking [V.S. Kropachev, V.P. Pogodin, et al.; ZASHCHITA METALLOV, Vol 28 No 2, Mar-Apr 92]	12
Determining the Tendency of 14Cr17Ni2 Steel to Intercrystallite Corrosion by an Accelerated Electrochemical Method [N.D. Tomashov, G.P. Chernova, et al.; ZASHCHITA METALLOV, Vol 28 No 2, Mar-Apr 92]	13
Measuring the Initial Rate of the Corrosion of Steel in High-Purity Water [L.N. Moskvina, A.A. Yefimov, et al.; ZASHCHITA METALLOV, Vol 28 No 2, Mar-Apr 92]	13
The Composition of the Surface of Corroded Ti-W Alloys [I.V. Kasatkina, R.Kh. Zalavutdinov, et al.; ZASHCHITA METALLOV, Vol 28 No 2, Mar-Apr 92]	14
The Effect of High-Temperature Thermomechanical Treatment on the Corrosion Cracking of Carbon Austenite Steel [Yu.N. Goykhenberg, M.A. Smirnov, et al.; ZASHCHITA METALLOV, Vol 28 No 2, Mar-Apr 92]	14
The Effect of HCl and Molasses on the Corrosion of 12Cr18Ni10Ti Steel in Phosphoric Acid Solutions [D.Kh. Kopeliovich, V.I. Ivlev, et al.; ZASHCHITA METALLOV, Vol 28 No 2, Mar-Apr 92]	15
Corrosion of Aluminum and the Alloy TsAM4-1 in a Nickel Plating Electrolyte [V.P. Artamonov; ZASHCHITA METALLOV, Vol 28 No 2, Mar-Apr 92]	15

Ferrous Metals

Thermodynamic Analysis of Processes Occurring During Molten Steel Pool Blasting With Gas-Oxygen Jet [T.G. Sabirzyanov, N.I. Globa, et al.; IZVESTIYA VYSSHIKH UCHEBNYKH ZAVEDENIY: CHERNAYA METALLURGIYA, No 1, Jan 92]	16
Characteristic Features of Hydrodynamic Processes During the Pulsation Treatment of Metal in a Casting Ladle [Yu.I. Shish, L.V. Rubin, et al.; ROSSIYSKAYA AKADEMIYA NAUK: SERIYA METALLY, No 1, Jan-Feb 92]	16
Increasing the Structural Strength of 20K Boiler Steel by Microalloying and Controlled Rolling [M.V. Bobylev, V.B. Kireyev, et al.; ROSSIYSKAYA AKADEMIYA NAUK: SERIYA METALLY, No 1, Jan-Feb 92]	16

The Effect of Alloying on the Kinetics of Carbide Particle Dissolution During the Laser Treatment of Steel [D.V. Shtanskiy, I.V. Lyasotskiy, et al.; ROSSIYSKAYA AKADEMIYA NAUK: SERIYA METALLY, No 1, Jan-Feb 92]	16
Peculiarities of Structural and Phase Transformations in Ion-Bombarded Inert Steels [O.V. Borodin, V.N. Voyevodin, et al.; FIZIKA I KHIMIYA OBRABOTKI MATERIALOV, No 1, Jan-Feb 92]	17
Controlling Steel and Alloy Structure During Suspension Inoculation by Ultradisperse High-Melting Compound Powders [V.P. Saburov, Ye.N. Khlystov, et al.; ROSSIYSKAYA AKADEMIYA NAUK: SERIYA METALLY, No 2, Mar-Apr 92]	17

Nonferrous Metals, Alloys, Brazes, Solders

Mechanism of Electron Excitation in Germanium by Atomic Hydrogen [V.F. Kharlamov; POVERKHNOST: FIZIKA, KHIMIYA, MEKHANIKA, No 1, Jan 92]	18
Effect of Electron Bombardment on Surface Charge of Alkali-Halogenide Crystals [B.G. Atabayev, N.N. Boltayev, et al.; POVERKHNOST: FIZIKA, KHIMIYA, MEKHANIKA, No 1, Jan 91]	18
Temperature-Dependent Concentration Profiles of Nitrogen Implanted in Be, Si, Fe, Nb [K.Sh. Chokin, Ye.Yu. Pereverzev; POVERKHNOST: FIZIKA, KHIMIYA, MEKHANIKA, No 1, Jan 92]	18
Unevenness of the Distribution of the Components of AKS Additive in Tungsten Wire [A.M. Bogomolov, A.A. Kalkov, et al.; ROSSIYSKAYA AKADEMIYA NAUK: SERIYA METALLY, No 1, Jan-Feb 92]	19
New Compounds With PuNi ₃ Structure in Rare Earth Metal-Cu-Al Systems [Yu.B. Kuzma, B.M. Stelmakhovich, et al.; ROSSIYSKAYA AKADEMIYA NAUK: SERIYA METALLY, No 2, Mar-Apr 92]	19
Vacuum Refining as Method of Producing High-Purity Aluminum [A.V. Vakhobov, F.U. Obidov, et al.; VYSOKOCHISTYYE VESHCHESTVA, No 2, Mar-Apr 92]	19
High-Purity Silicon for Ionizing Radiation Detectors [K.N. Neymark, Yu.V. Trubitsyn, et al.; VYSOKOCHISTYYE VESHCHESTVA, No 2, Mar-Apr 92]	20
Today's State of High-Purity Metal Fluoride Production for Fiber Optics [V.I. Zvereva; VYSOKOCHISTYYE VESHCHESTVA, No 2, Mar-Apr 92]	20
High-Purity Silane Silicon-Based Ionizing Radiation Detectors [Yu.A. Nechuneyev, G.V. Ladonychev, et al.; VYSOKOCHISTYYE VESHCHESTVA, No 2, Mar-Apr 92]	20

Nonmetallic Materials

Effect of Pulsed Heat Treatment on Electrophysical Properties of Zr-Si Interface [A.M. Chaplanov, A.N. Shibko, et al.; POVERKHNOST: FIZIKA, KHIMIYA, MEKHANIKA, No 1, Jan 92]	21
Photochemical Etching of Silicon With Continuous-Wave Laser Radiation [Ye.A. Volkova, A.M. Popos, et al.; POVERKHNOST: FIZIKA, KHIMIYA, MEKHANIKA, No 1, Jan 92]	21
Dependence of Nonhomogeneity of Thin Glass Films Produced by High-Frequency Sputtering on Chemical Composition of Substrate Glass [I.S. Malashchenko, V.P. Redko, et al.; POVERKHNOST: FIZIKA, KHIMIYA, MEKHANIKA, No 1, Jan 92]	21
Change in Properties of Carbon Materials Under Neutron Bombardment [Yu.S. Virgilyev; FIZIKA I KHIMIYA OBRABOTKI MATERIALOV, No 1, Jan-Feb 92]	22
Structural Changes on Silicon Surface Under Laser Radiation [A.F. Banishev, M.M. Novikov; FIZIKA I KHIMIYA OBRABOTKI MATERIALOV, No 1, Jan-Feb 92]	22
Properties of Molten Slag in Thermal Reprocessing of Radioactive Waste on Base of Shaft Furnace [S.A. Dmitriyev, S.V. Stefanovskiy, et al.; FIZIKA I KHIMIYA OBRABOTKI MATERIALOV, No 1, Jan-Feb 92]	23
'Dry' Photoanodic Microtreatment of Semiconductors With Laser Beam [D.T. Alimov, V.M. Kosov, et al.; FIZIKA I KHIMIYA OBRABOTKI MATERIALOV, No 1, Jan-Feb 92]	23

Removing Freon-14 Microimpurity From Krypton by Adsorption [T.A. Kuznetsova, Ye.N. Yegorov, et al.; VYSOKOCHISTYYE VESHCHESTVA, No 2, Mar-Apr 92]	23
Removing Oxygen Impurity From Tellurium Used for Optical Material Synthesis [A.B. Lobanov, K.A. Pavlova, et al.; VYSOKOCHISTYYE VESHCHESTVA, No 2, Mar-Apr 92]	24

Preparations

Chemical Reaction of Copper Sulfate With a Collective Copper-Zinc Concentrate [N.V. Serova, M.P. Lysykh, et al.; ROSSIYSKAYA AKADEMIYA NAUK: SERIYA METALLY, No 1, Jan-Feb 92]	25
The Theory and Practice of the Transfer of Ultrasound Vibrations to Molten Metal Through a Waveguide Wire [I.I. Safronov, I.A. Leurda; ROSSIYSKAYA AKADEMIYA NAUK: SERIYA METALLY, No 1, Jan-Feb 92]	25
Properties and Use of Uranium-Fluorine Plasma. Part 2: Recovery of Uranium from UF ₆ Without Reactants in High-Frequency Discharge Without Electrodes Discharge [Yu.N. Tumanov, K.V. Tsirelnikov; FIZIKA I KHIMIYA OBRABOTKI MATERIALOV, No 1, Jan-Feb 92]	25
Investigation of Mechanical Properties of NiAl-Based Materials Produced by Self-Propagating High-Temperature Synthesis Method [A.G. Nikolayev, V.G. Koshelyayeva, et al.; ROSSIYSKAYA AKADEMIYA NAUK: SERIYA METALLY, No 2, Mar-Apr 92]	26
Powder Titanium Oxidation During Heating in Air Medium [V.V. Tavgen, Ye.V. Shinkareva, et al.; POROSHKOVAYA METALLURGIYA, No 3(351), Mar 92]	26
Effect of Structure on Deformation of Metal Fabric for Composite Reinforcement [L.R. Vishnyakov, L.I. Feodosyeva, et al.; POROSHKOVAYA METALLURGIYA, No 3 (351), Mar 92]	27
Hot Extrusion of Aluminum Alloy Granules in Two-High Rolling Mill [V.N. Kornilov, N.V. Shepelskiy; POROSHKOVAYA METALLURGIYA, No 3 (351), Mar 92]	27
Porous Copper-Based Fibrous Powder Materials [M.V. Tumilovich, A.G. Kostornov, et al.; POROSHKOVAYA METALLURGIYA, No 3 (351), Mar 92]	27
Structure Formation and Electric Conductivity in Thick Disperse Ni ₃ B Powder-Based Films [Yu.K. Kulba, B.M. Rud, et al.; POROSHKOVAYA METALLURGIYA, No 3 (351), Mar 92]	27
Effect of Electrode Composite Materials' Composition and Structure on Their Erosion Character and Discharge Dynamics in Railtron [V.P. Zinovyeva, A.D. Lebedev, et al.; POROSHKOVAYA METALLURGIYA, No 3 (351), Mar 92]	28
Experience of Making Hard Alloy Cutting Tools by Self-Propagating High-Temperature Synthesis Method [S.M. Vaytsekhovich, A.A. Mishulin; POROSHKOVAYA METALLURGIYA, No 3 (351), Mar 92]	28
Dynamics of Multistage Purification by Zone Recrystallization [G.G. Devyatikh, V.A. Dozorov, et al.; VYSOKOCHISTYYE VESHCHESTVA, No 2, Mar-Apr 92]	28

Treatments

Calculated and Experimental Estimates of the Parameters of the Activation of Alloys Based on Aluminum and Vanadium by the Neutrons of Fission and Synthesis Reactors [L.I. Ivanov, V.V. Ivanov, et al.; ROSSIYSKAYA AKADEMIYA NAUK: SERIYA METALLY, No 1, Jan-Feb 92]	30
Thermal Impact Loading of Metal by Pulsed Proton Beam [V.I. Boyko, I.V. Shamanin, et al.; FIZIKA I KHIMIYA OBRABOTKI MATERIALOV, No 1, Jan-Feb 92]	30
Effect of Hardening Conditions on Mechanical Properties and Residual Stresses in High-Temperature EP962 Nickel Alloys [V.I. Yermenko, N.N. Korneyeva, et al.; METALLOVEDENIYE I TERMICHESKAYA OBRABOTKA METALLOV, No 1, Jan 92]	31
Effect of Straining Conditions in (α+β)-Area on Structure and Properties of Titanium Pseudo-α-Alloy [I.N. Razuwayeva, V.N. Kopylov, et al.; METALLOVEDENIYE I TERMICHESKAYA OBRABOTKA METALLOV, No 1, Jan 92]	31
Effect of Aging on Structure and Elastic Properties of Hardened (α+β) Titanium Alloys [T.A. Panayoti, A.S. Gorbova (deceased), et al.; METALLOVEDENIYE I TERMICHESKAYA OBRABOTKA METALLOV, No 1, Jan 92]	31

- Improving Properties of Large Semifinished Items From VT23 Alloy by Thermal Cycling
[V.S. Lyasotskaya, A.I. Khorev, et al.; *METALLOVEDENIYE I TERMICHESKAYA OBRABOTKA METALLOV*, No 1, Jan 92] 32
- On Possibility of Removing Fluorine From Silicon Nitride Powder Surface by Chemical Reagents
[G.N. Komratov, Yu.M. Shulga; *POROSHKOVAYA METALLURGIYA*, No 3 (351), Mar 92] 32

Extractive Metallurgy, Mining

- Selected Features of the Interconnection of the Genesis, Chemicomineralogic Makeup, and Reducibility of Manganese Ore Materials From Different Deposits. Part 4: Selected Characteristic Features of the Mechanism of the Carbon Reduction of Manganese Ore Materials
[S.G. Grishchenko, T.F. Raychenko, et al.; *ROSSIYSKAYA AKADEMIYA NAUK: SERIYA METALLY*, No 1, Jan-Feb 92] 33

Miscellaneous

- Reagent-Free Fluorine-Containing Waste Water Treatment
[B.L. Prisyazhnyuk; *STEKLO I KERAMIKA*, No 1, Jan 92] 34

Electron Emission From Metals Bombarded by Fast Multiple-Charge Ions

927D0157A Moscow *POVERKHNOST: FIZIKA, KHIMIYA, MEKHANIKA* in Russian No 1, Jan 92 (manuscript received 28 Sep 90, signed to press 26 Oct 90) pp 5-11 [Article by V.V. Katin, Yu.V. Martynenko, and Yu.N. Yavlinskiy, Institute of Atomic Energy imeni I.V. Kurchatov, Moscow; UDC 539.09.082]

[Abstract] Electron emission from the metal surface under vacuum due to its bombardment by fast multiple-charge ions is analyzed theoretically for the effect of the space charge, considering that the electrons leaving the surface establish an electric field which impedes further emission so that an electric double layer is formed. This electric double layer and kinetics of its formation have been described by a model based on the Boltzmann equation ($\nabla \cdot \mathbf{f} + (eF/m)(\delta f/\delta v) = 0$ (e - electron charge, m - electron mass), assuming that the transient period of space charge buildup is much shorter than the characteristic time of evolution of the electron excitation region near the metal surface within which the electron velocity distribution function $f(v)$ satisfies that equation. In that equation F denotes the electric field intensity vector $\nabla F = -4\pi e \int (f_1 + f_2)dv$, where f_1 is the distribution function of electrons moving from the surface ($v_x > 0$), f_2 - distribution function of electrons moving to the surface ($v_x < 0$) or at rest ($v_x = 0$), and v_x is the electron velocity in the direction normal to the surface. At the metal-vacuum interface $f_1(v) = f_0(v)$, where $f_0(v)$ is the distribution function of electrons leaving the surface. From the Boltzmann equation and that expression for ∇F is derived an equation for the electric potential ϕ which electron emission establishes within the region $x \geq 0$ just above the surface:

$$\frac{\partial^2 \phi}{\partial x^2} = 8\pi e \int_{(2e\phi/m)^{1/2}}^{\infty} \frac{f_0(v) v_x dv_x dv_y dv_z}{[v_x^2 - (2e\phi/m)]^{3/2}}.$$

This equation is solved for the maximum electric potential, in the quasi-static approximation of an electron cloud adjusted to temperature changes. The results of calculations based on the classical theory of primary shower and thermal peak, and including slowdown action by the space charge, do not fit known experimental data. The experimental evidence is shown to be more predictable by consideration of an Auger shower within the region of strong electron excitation as the mechanism of electron emission from a metal surface, when fast multiple-charge ions penetrating the metal target lose their energy during inelastic collisions against metal atoms and impart it to the electronic subsystem of these atoms (about 20-30 keV/nm). The electric field gradient dE/dx under these conditions is calculated according to Bohr's relation, this gradient being the sum of two parts: one (approximately 65 percent) representing the energy received almost instantaneously and carried away by secondary electrons and one part (approximately 35 percent) representing the energy stored in vacant shells of metal ions over a much longer period of time. This model confirms experimental data

indicating an only weak dependence of the electron emission coefficient ($K \approx 200$) on the work function of the metal. This dependence would be exponential and thus strong according to the thermal peak model, because this model as well and the primary shower model do not account for slowdown of electron further electron emission by the electron cloud already formed above the metal surface. References 15.

Enthalpy of the Formation of Melts of the System Cr-Si-C

927D0158D Moscow *ROSSIYSKAYA AKADEMIYA NAUK: SERIYA METALLY* in Russian No 1, Jan-Feb 92 (manuscript received 27 Nov 90) pp 49-52

[Article by V.T. Vitusevich, Kiev; UDC 536.653.722:669.26'782'784-154]

[Abstract] The author of the study reported herein worked to experimentally determine the partial and integral enthalpies of the formation of liquid alloys of the system Cr-Si-C throughout the entire range of the existence of homogeneous compositions at a temperature of 2,160 \pm 20 K. Electrolytic chromium, type KEF 12/0.5 semiconductor monocrystalline silicon, and spectrally pure graphite were used to prepare the study melts. The chromium contained the following impurities (percent by mass): C, 0.08; O, 0.03; N, 0.002; Cu < 0.001; and Mo < 0.01. All of the calorimetric measurements were taken in an atmosphere of purified type B (TU 51-940-80) helium. A low-temperature calorimeter was used in accordance with a procedure detailed elsewhere. The enthalpies of the components' heating were borrowed from published reference manuals. The partial enthalpies of the aforesaid three-component alloys were measured for the following radial sections (X_{Si}/X_{Cr}): 0.1/0.9; 0.2/0.8; 0.33/0.67; 0.46/0.54; 0.5/0.5; and 0.83/0.17. The partial enthalpies of mixing (ΔH_i) plotted were overall found to be analogous to those of the three-component system Fe-Si-C. Two regions of compositions distinguished by the nature of their interatomic interaction were quite evident. In liquid alloys rich in a 3d-metal, ΔH_i changed sharply as the contents of both silicon and carbon were increased. In melts enriched in silicon, on the other hand, carbon was found to have virtually no effect on ΔH_i . The previously discovered distinction in the partial functions of Cr-C melts associated with their microinhomogeneity as also noted in the dependences of the enthalpies of the three-component melts examined here. The said distinction was found to disappear only when the silicon content rose to more than 20 atomic percent. The change in the initial partial enthalpies of the dissolution of graphite as a function of the silicon content in the starting melts was found to be extremal with a positive deviation from the additive values. The experiments performed confirmed that like binary alloys of the system Cr-Si, three-component alloys are characterized by an intensive interaction between their different types of atoms. The partial enthalpies of the formation of the components of melts of the system Cr-Si-C are detailed in a table. Figures 2; table 1; references 9: Russian.

Oxide Formation in Chromium Condensates at Elevated Temperatures

927D0158E Moscow ROSSIYSKAYA AKADEMIYA
NAUK: SERIYA METALLY in Russian No 1,
Jan-Feb 92 (manuscript received 30 Jul 90) pp 69-70

[Article by M.V. Belous, L.P. Germash, I.Ye. Kotenko,
and S.I. Sidorenko, Kiev; UDC 669.017.3:536.423.4]

[Abstract] The authors of this concise report studied the effect of annealing temperature on the structure and phase composition of chromium condensates produced by thermoionic precipitation versus the properties of films produced by resistive and electron beam vaporization. The study condensates were subjected to roentgenographic analysis on a DRON-2.0 diffractometer and URS-2.0 unit in iron and copper radiation. Electronographic studies were conducted on an EMR-100 electronograph with an accelerating voltage of 75 kV, and the structure of the condensates was studied with an EMR-100L transmission electron microscope in a vacuum of 3×10^{-3} Pa with an accelerating voltage of 75 to 100 kV. An M-1305 mass spectrometer equipped with an ion bombardment attachment was used to perform a layer-by-layer analysis of the study condensates. The structure of the chromium condensates produced by thermoionic precipitation proved to be the most interesting. Only a chromium line was found to be present in their electronograms. Their electronograms also exhibited distinct texture maxima that were arranged in slightly fuzzy diffraction rings. The condensates manifested a type (110) texture. As the voltage on the substrate was increased to -3 kV, the fuzziness of the diffraction rings decreased, and a type (111) texture appeared. At substrate temperatures of 470, 570, and 670 K, the condensates contained only pure chromium as before. At the same time, however, the application of voltage to the substrate resulted in a worsening of the conditions of oriented condensation in isolated cases. The chromium condensates precipitated by the resistive technique contained Cr_3O_4 and Cr_3O along with pure chromium. No signs of texture or epitaxy were evident in the said condensates. The chromium condensates produced by the electron beam method were characterized by the presence of wide diffraction lines, which was taken as an indication of the high crystal dispersivity. A line indicating the suboxide Cr_3O was evident against the background of strong and wide diffraction lines from the body-centered crystal lattice of the chromium. This effect was more pronounced during condensation on a substrate at room temperature. The chromium condensates oxidized during annealing. The suboxide Cr_3O disappeared upon heating to 670 K, and Cr_3O_4 formed in its place. At 870 K, the latter transformed into Cr_2O_3 . The lattice period of the chromium of the condensates formed by the thermoionic method was somewhat larger than that of the condensates produced by resistive and electron-beam precipitation. This was taken as confirmation of the fact that the films produced by the thermoionic method contain fewer impurities than do the chromium condensates produced by the other methods. All of the films studied contained more oxygen in their surface layers than in their bulk. The films produced by the thermoionic method contained less

oxygen than the others, however. The films' oxygen content diminished as the substrate temperature was increased.

New Phenomenon in Solid Material Under Compression to Ultrahigh Pressure

927D0159I Moscow FIZIKA I KHIMIYA OBRABOTKI
MATERIALOV in Russian No 1, Jan-Feb 92
(manuscript received 25 Oct 90) pp 121-125 [Article by
V.A. Shapochkin and Ye.V. Shapochkina, Moscow;
UDC 539.3/8:621.791]

[Abstract] Transition from plastic to purely elastic deformation of a solid material under compression by rigid plungers or punches is described, this heretofore unknown phenomenon occurring as the pressure rises from high levels (up to 100 kbar) to ultrahigh levels (up to several Mbar) and not conforming to classical mechanics of deformable media. As the pressure rises to high levels (up to 100 kbar), external friction between the plungers and the deformable solid material reaches the magnitude of internal friction in that material. This is caused by a combination of mechanical and physicochemical processes. As the pressure then rises to ultrahigh levels (up to 1 Mbar and higher), "outflow" of the compressed medium through the clearance between plungers ceases as the clearance closes so that a cavity forms and the pressure on the material in it becomes hydrostatic. The attendant transition to elastic deformation, while peculiar to high and ultrahigh pressures only, is universal with regard to physical and mechanical behavior of the deformable material between plungers with contact surfaces of any shape. Following initial elastoplastic deformation, convex contact surfaces were found to become flat and the solid material to cease deforming plastically as the pressure reached some critical level. Flat contact surfaces were found to become concave and concave contact surfaces, following initial "outflow" of the deformable solid material, to eventually bend so as to create a closed cavity with the material inside continuing to deform elastically only. This was consistently observed in industrial production of synthetic diamonds in high-pressure chambers with concave plungers. Laboratory experiments confirming this phenomenon were performed with flat plungers made of VK-4/6/8 W-Co alloys and thus having a high compressive strength (up to 5000 kN/mm²). On the basis of this phenomenon has been developed a new method of producing synthetic diamonds, namely by "contact pressures". Figures 1; references 25.

Fracture Analysis of Cast Steel and Pig Iron From Synergetic Viewpoint

927D0163A Moscow ROSSIYSKAYA AKADEMIYA
NAUK: SERIYA METALLY in Russian No 2,
Mar-Apr 92 pp 57-63

[Article by I.P. Volchok, O.B. Kolotilkin, Zaporozhye;
UDC 669.141.246+669.13]:620.192.7]

[Abstract] Metal failure—multistage and multilevel relaxation processes in which various structural elements successively participate—are described from the synergetic

viewpoint, and the cast steel and pig iron fracture process is analyzed. It is shown that during fracture, the steel and iron structure change according to the law of dissipative systems whereby the nonmetallic and graphite inclusions play a dominant role. Dislocation, slip line, and microcrack fluctuations are observed in the vicinity of these inclusions. These inclusions serve as stress concentrators in the matrix and determine the position of bifurcation points. The dependence of the mechanical properties of steel 35L on the type of inclusions and their index and fracture indicators of steel 35L at a 12 percent residual deformation are computed, and the effect of the testing temperature on the number of total and inclusion-bound microcracks, the effect of the graphite shape parameter and index on the pig iron tensile and bending strength and hardness, and the dependence of toughness and thermal stability, cast iron dissolution rate in molten glass, and the tool friction surface roughness on the graphite shape parameter and index are plotted. Erosion failure of the pig iron surface under the effect of a molten glass body is examined. An analysis of the findings indicates that from the viewpoint of mechanical properties, toughness, and thermal stability, globular graphite is optimal. Pig iron with vermicular graphite has the highest resistance to erosion failure in a molten glass body. Figures 4; tables 2; references 11.

Laser Probing of Initial Stage of $\gamma \rightarrow \alpha$ Martensite Transformation

927D0163B Moscow ROSSIYSKAYA AKADEMIYA
NAUK: SERIYA METALLY in Russian No 2,
Mar-Apr 92 pp 105-108

[Article by M.P. Kashchenko, V.V. Letuchev, S.V. Konov-
alov, S.V. Neskromnyy, Yekaterinburg; UDC
669.112.227.346.2]

[Abstract] In iron-based alloys, $\gamma \rightarrow \alpha$ martensite transformation (MP), which occurs under largely nonequilibrium conditions by means of rapid lattice reordering and displays clear signs of a first-kind phase transition is discussed; the task of probing the first stage of martensite transformation by picosecond laser radiation pulses in order to investigate the martensite crystal nucleation process is formulated on the basis of the findings obtained in the framework of the concept of dislocation-induced nucleation and wave-controlled growth of α -martensite. It is assumed that rectilinear mixed austenite dislocations serve as nucleation centers of individual martensite transformations; that there is a one-to-one correspondence between the dislocation characteristics; and that the process of $\gamma \rightarrow \alpha$ martensite transformation starts with the appearance of an excited lattice state. Single crystals of a Fe+31.5 percent Ni alloy with a close to (100)_γ plane are used in the study. A block diagram of the experimental unit is presented and the sample surface after the transformation is photographed under a x600 magnification. The findings play a fundamental role in understanding the origins of martensite transformation in that they show that interpretation of the dynamic structure of the excited lattice state in the nonequilibrium area of the nonlinear transformation wave is the key to comprehending the

processes which control the growth of the new phase during reconstructive cooperative restructuring. Figures 2; references 9.

Change in Hydrogen Solubility in Metals at Melting Point

927D0163E Moscow ROSSIYSKAYA AKADEMIYA
NAUK: SERIYA METALLY in Russian No 2,
Mar-Apr 92 pp 187-190

[Article by V.I. Lakomskiy, Zaporozhye; UDC
669.046.552.3]

[Abstract] An abrupt increase in the gas solubility in metal at the melting point at which not only the state of aggregation, but also the heat content, molar volume, and entropy as well as thermoelectromotive force, conductivity, and magnetic susceptibility change in the metal is discussed, and it is assumed that at the solid metal's melting point, two phases of the single-component system exist simultaneously: a solid and a liquid. It is further assumed that the gas dissolved in the solid metal and the gas dissolved in the metallic melt are in equilibrium with the gas in the gaseous phase at the melting point. An expression is derived for calculating the change in the hydrogen solubility in a pure metal at its melting point on the basis of thermodynamic partial parameters of the liquid and solid metallic solutions. Analytical and experimental data on the hydrogen solubility jump in a number of metals at their melting point are compared. It is emphasized that the analytical formula is suitable for other metal-gas systems if they do not form strong chemical compounds near the melting point. Tables 1; references 12: 8 Russian, 4 Western.

Thermodynamic Properties of Fe-Ni-O and Fe-Ni-O-Ta-Si System Melts

927D0163I Moscow ROSSIYSKAYA AKADEMIYA
NAUK: SERIYA METALLY in Russian No 2,
Mar-Apr 92 pp 233-235

[Article by V.S. Sudavtsova, N.O. Sharkina, Kiev; UDC
541.122]

[Abstract] The role of oxygen in the development of nonmetallic inclusions of various compositions and pores and cracks which worsen the mechanical, operating, and other properties of metals and alloys in the solid state and metal products are discussed, and an attempt to determine the thermochemical properties of Fe-Ni-O and Fe-Ni-O-Ta-Si system melts by calorimetry methods is reported. The NiO dissolution enthalpy in a liquid alloy consisting of 64 percent Fe and 36 percent Ni and partial molar enthalpies of Ta in melts of the Fe-Ni-O system and Si in Fe-Ni-O-Ta systems are measured in an isoperibolic calorimeter. The resulting partial enthalpies of component mixing are used for calculating the oxygen, tantalum, and silicon activities in a regular solution approximation. The results show that partial oxygen mixing enthalpies are characterized by very high negative values while partial enthalpies of Si mixing in Fe-Ni-O-Ta-Si systems are close to those obtained for Fe-S and Ni-S systems, attesting to the fact that Si does not interact with the dissolved oxygen

remaining after the Fe-Ni-O melt deoxidation with tantalum. It is shown that indirect conclusions about the deoxidizing properties of various elements or their complexes may be drawn from thermochemical data. Tables 1; references 4.

Role of Plastic Deformation in Structure Formation of Ceramic Materials

927D0164J Kiev *POROSHKOVAYA METALLURGIYA* in Russian No 3 (351), Mar 92 pp 80-88

[Article by G.S. Oleynik, Institute of Materials Science Problems at the Ukrainian Academy of Sciences, Kiev; UDC 669.018.45:539.5]

[Abstract] The use of plastic deformation as a process of structural reordering in ceramic materials whereby the ceramics may be deformed by many types of mechanical working traditionally used in metallurgy is reviewed on the basis of numerous foreign and domestic sources, and it is stressed that plastic working of ceramics has not yet gained due recognition. An analysis of recent publications shows that the microstructure of covalent type ceramic materials can be controlled by processes of plastic deformation realized at the stage of powder preparation and subsequent sintering and compaction. Together with the emerging trends in the development of ceramic technologies, particularly the use of high pressures in all phases of material production, including dynamic compression and molding of materials in the superplasticity state, make it possible to conclude that deformation working may soon become widely used for oriented change in the structural state of ceramic materials. Tables 2; references 68: 30 Russian, 38 Western.

Resistance of Titanium Carbide Powders Synthesized by Various Methods to H_2O_2 and H_2SO_4 Solutions

927D0164L Kiev *POROSHKOVAYA METALLURGIYA* in Russian No 3 (351), Mar 92 pp 102-105

[Article by G.N. Komratov, I.D. Chausskaya, Structural Macrokinetics Institute at Russia's Academy of Sciences, Chernogolovka; UDC 546.261:620.193]

[Abstract] The effect of the titanium carbide (KT) powder synthesis method and original products on the chemical, physical, and mechanical properties of the powders and their resistance to hydrogen peroxide and sulfuric acid solutions are investigated; to this end, TiC powders produced by furnace synthesis, pseudofusion, and self-propagating high-temperature synthesis are tested. The chemical composition of the powders and its variation ranges as well as the specific surface as a function of synthesis method are summarized and the TiC powder microstructure is examined under an electron microscope and JCSA-733 X-ray microanalyzer. The TiC particle size distribution and the coefficient of TiC powder decomposition process rate are computed and the kinetic curves of titanium ion accumulation in the solution during the TiC powder decomposition process at 80 and 40 °C are plotted. The TiC powder decomposition activation energy in H_2O_2

and H_2SO_4 as a function of synthesis method is summarized. An analysis shows that the titanium carbide powder decomposition rate in the acid and peroxide solutions depends primarily on the solid material surface area, which is a function of the titanium carbide production and treatment methods. Figures 2; tables 4; references 5.

On Problem of Lowering Light Absorption by Films in Infrared Spectrum

927D0165B Moscow *VYSOKOCHISTYYE VESHCHESTVA* in Russian No 2, Mar-Apr 92 pp 34-40

[Article by Ye.N. Kotlov, D.N. Gromov, V.A. Ivanov, I.I. Kovalenko, M.N. Kulbitskaya, V.N. Prokashchev, B.F. Shifrin, D.Ye. Pogarev, Leningrad Avionics Institute; UDC 535.81:539.238:537.311.33]

[Abstract] The effect of the absorptance and refractive index of films on the properties of interference coats made from them and ways of decreasing the light absorption by such films by selecting the most chemically pure initial materials and optimum temperature conditions of the deposition process are discussed, and absorption by ZnSe, ZnS, BaF_2 , PbF_2 , SrF_2 , and NaF films on a 10.6 μm wavelength produced with the help of various chemical reagents is investigated. The film deposition method is outlined, and the refractive indices of films and single crystals and the relative density of films are summarized. Absorption is measured by the calorimetry method. The dependence of the barium fluoride film absorptance on the substrate temperature during the deposition and the transmission, reflection, and absorption spectra of the lead fluoride film on a zinc selenide substrate are plotted. The film absorptance on a 10.6 μm wavelength as a function of the substrate temperature during the deposition is summarized. An analysis demonstrates that in order to lower the light absorption by films and narrow its spread, it is necessary to use either single crystal or optical ceramic source materials; porosity is shown to have a significant effect on absorptance in the case of chemically pure substances. The lower the film density, the more water it absorbs and the more infrared light it absorbs. The study indicates that there is a temperature optimum for reducing absorption; films produced at the optimum temperature have a definite polycrystalline structure, i.e., are the most dense. Figures 3; tables 2; references 8: 4 Russian, 4 Western.

Tandem Laser-Probe Mass-Reflectron

927D0165I Moscow *VYSOKOCHISTYYE VESHCHESTVA* in Russian No 2, Mar-Apr 92 pp 168-172

[Article by I.D. Kovalev, P.A. Shmonin, High-Purity Substance Chemistry Institute at Russia's Academy of Sciences, Nizhny Novgorod; UDC 621.384.8]

[Abstract] The use of laser probe mass-spectrometers with a time of flight analyzers in microelectronics, biology, and medicine as well as for determining the impurity distribution in solids is discussed, and a laser-probe mass-spectrometer with free laser plasma scattering in which two

mass-reflectron-type mass analyzers are assembled in series is described. A schematic diagram of the device is cited, and its operating principle is outlined in detail. The specimen is handled by ShDR-721 step motors whose operation is synchronized with laser pulses and is controlled by an IBM PC/XT microcomputer. The background emission level is determined by the detector's intrinsic noise and the scattered base ions, i.e., scattering by the residual gas, analyzer electrodes, and vacuum chamber walls. The ion beam reflected by the specimen under study is purified so as to filter out the base ions. The detector's geometric transmission factor is 10^{-7} , and its detection threshold is $5 \cdot 10^{-7}$

percent measured in the digital signal accumulation mode on the basis of $2 \cdot 10^{10}$ ions counted in one hour. The detection threshold may be lowered by reducing the scattered ion background. It is expected that a 4K-channel time analyzer consisting of a time-to-code converter with a 20 ns resolution and an IBM PC/XT on-line microcomputer ensuring a spectrum composition at a 50 Hz frequency will be used for recording the mass spectrum. Recording of the total number of ions and the analytical line profile together with the use of digital filtering methods will make it possible further to lower the detection threshold by an order of magnitude. Figures 1; references 8: 6 Russian, 2 Western.

Porosity and Protective Action of Aluminum Galvanic Coatings

927D0155E Moscow ZASHCHITA METALLOV
in Russian Vol 28 No 1, Jan-Feb 92 pp 125-128

[Abstract of article by V. V. Krasnoyarskiy, V. A. Mazin, T. I. Zhukova, S. A. Smirnova, and V. A. Kazakov, Institute of Physical Chemistry, USSR Academy of Sciences; UDC 620.193.2]

[Abstract] The porosity and corrosion resistance of galvanic aluminum coatings were studied. The coatings were applied to flat disk-shaped substrates 30 mm in diameter, which were made from St3 carbon steel or copper. The coatings were applied from electrolytes of standard composition: alkylaluminum based on $\text{Al}(\text{C}_2\text{H}_5)_3$, NaF, and toluene; alkylbenzene based on AlBr_3 and ethylbenzene; and ether-hydride based on AlCl_3 , LiAlH_4 , and butylene oxide. Coating thickness varied from 5 to 30 μm and was controlled by a magnetic thickness gauge to within $\pm 3 \mu\text{m}$. Porosity was determined electrochemically. A sharp drop in coating porosity was observed when coating thickness reached 5 to 7 μm , after which porosity was not appreciably affected. Coatings obtained from the ether-hydride and alkylaluminum electrolytes imparted the best protective properties. There was also a surprisingly strong relationship between coating porosity and the type of electrolyte used in conjunction with a particular substrate material. For example, the porosity of a coating 5 μm thick applied to a copper substrate from the ether-hydride electrolyte was about 6 percent, but it was less than 0.01 percent on the steel substrate. Porosity could also be reduced several fold by anodizing the coatings and then filling them in with an oxide film and painting them with an inorganic paint. Corrosion resistance was measured from the drop in coating potential during long-term testing of specimens in a three percent solution of NaCl. Coatings applied from alkylaluminum electrolyte to a copper substrate protected the substrate for 300 to 8000 hours, depending on coating thickness. Similar findings were obtained for the steel substrates. Figures 2; references 9: 5 Russian, 4 Western.

Role of Hydrogen in the Formation of Silky Mat Coatings

927D0156L Moscow ZASHCHITA METALLOV
in Russian Vol 28 No 2, Mar-Apr 92 (manuscript received 6 Apr 89) pp 326-331

[Article by S.S. Kruglikov, N.G. Bakhchisaraytsyan, and M.A. Pevzner, Moscow Chemical Technology Institute imeni D.I. Mendeleev; UDC 621.357.7:669.248]

[Abstract] Silky mat nickel coatings are produced by precipitating nickel from electrolyte emulsions. Silky mat coatings are formed as follows: Particles of the organic phase in the form of emulsion drops periodically come into direct contact with the cathode surface, which results in a cessation of the process of electrodeposition onto the respective segment of the surface. Along with organic phase particles, the electrolyte absolutely must contain a brightener (such as saccharin) to prevent the formation of a crystalline relief. In the presence of a brightener, the

periodic stopping and starting of the process of nickel precipitation under the effect of disperse-phase particles results in a roughness consisting of microirregularities that are very different from those of the crystalline roughness of mat nickel precipitates. In order to discover possible ways of controlling the formation of silky mat coatings, the authors of this concise report studied the behavior of a preliminarily dyed disperse phase in the volume of an electrolyte and on a cathode surface under different electrolysis conditions. Their studies were based on microscopic observations of still and motion-picture photographs. The studies performed indicated the need for continuous regeneration of the electrolyte by passing it through a cooler (temperature, 25 to 30°) and then through a heater. A total of 10 different electrolytes were tested. Two sulfate-acetate electrolytes with a relatively low partial current density of hydrogen evolution were found to result in silky mat coatings with a surface roughness (R_a) of $>0.2 \mu\text{m}$, which confirmed the authors' hypothesis that hydrogen plays a role in the formation of silky mat coatings. The first of the two aforesaid electrolytes contained the following (mol/l): $\text{Ni}(\text{CH}_3\text{COO})_2 \cdot 4\text{H}_2\text{O}$, 0.175; $\text{NiCl}_2 \cdot 6\text{H}_2\text{O}$, 0.125; and $\text{NiSO}_4 \cdot 7\text{H}_2\text{O}$, 0.5. The second electrolyte contained the following (mol/l): $\text{Ni}(\text{CH}_3\text{COO})_2 \cdot 4\text{H}_2\text{O}$, 0.08; $\text{NiCl}_2 \cdot 6\text{H}_2\text{O}$, 0.2; and $\text{NiSO}_4 \cdot 7\text{H}_2\text{O}$, 0.22. Further tests confirmed that both of the said electrolytes may be used continuously without regeneration in a two-shift regimen (12 hours at a time) and still result in silky mat coatings with an acceptable surface roughness ($R_a = 0.25$ to $0.30 \mu\text{m}$). The first of the two aforesaid electrolytes has passed commercial tests and is now being used at two enterprises. Figures 2; table 1; references 2: Russian.

Laser-Stimulated Electrodeposition of a Tin-Bismuth Alloy

927D0156M Moscow ZASHCHITA METALLOV
in Russian Vol 28 No 2, Mar-Apr 92 (manuscript received 11 Nov 90) pp 334-337

[Article by Yu.V. Seryanov and L.V. Aravina; UDC 621.793.14]

[Abstract] In a continuation of their previously reported research, the authors of this concise report have studied the laser-stimulated electrodeposition of tin-bismuth alloys. As a working electrolyte, they used a mixture of the following (g/l with no allowance for the recrystallization of water): SnSO_4 , 50; $\text{Bi}(\text{NO}_3)_3$, 1; H_2SO_4 , 100; NaCl, 0.5; and OS20, 5. A horizontally oriented copper foil was used as the cathode, and a tin foil was used as the anode. Saturated silver chloride was used as the standard electrode. A laser electrochemical unit based on an LTN-102 laser ($\lambda = 1.06 \mu\text{m}$, $P \leq 120 \text{ W}$) was used for the experiments in accordance with a procedure detailed elsewhere. X-ray phase and chemical analysis were used to determine the composition of the resultant coatings, and electron microscopy photography was used to study the coating surfaces. On the basis of their experiments and calculations, the authors concluded that laser-stimulated electrodeposition of a tin-bismuth alloy under optimal conditions ($E' = -0.76 \text{ V}$, $W' = 21 \text{ kW/cm}^2$, $\lambda = 1.06 \mu\text{m}$) is

a suitable technique for restoring the defects of a protective coating or for applying microdoses of solder to small elements of the topology of printed circuit boards and hybrid integrated circuits. Figures 2; references 6: Russian.

Effect of Organic Surfactants on the Composition of Galvanic Alloys

927D0156N Moscow ZASHCHITA METALLOV in Russian Vol 28 No 2, Mar-Apr 92 (manuscript received 29 Oct 90) pp 337-338

[Article by Yu.P. Perelygin; UDC 621.357.7]

[Abstract] The author of this concise report worked to establish the mathematical dependence of an alloy's composition on the concentration of surfactant used during electrolysis, provided that all other conditions remain equal. The study was conducted at room temperature, with a current density of 100 A/m², and with an electrolyte with the following composition (kg/m³): cadmium sulfate, 5; indium sulfate, 15; sodium bitartrate, 100; and sodium sulfate, 20. The electrolyte had a pH of 4.0. The preparation OS-20 was used as an organic surfactant in amounts of 0.5, 0.7, 0.8, and 1.0 kg/m³, and the content of indium in the study alloy specimens amounted to 43, 66, 70, and 82 percent (by mass), respectively. A program introduced elsewhere that was based on the least squares method was used to process the results. The said program enabled the author to establish (with a 0.998 correlation coefficient) that the data obtained from the experiments may be described by the following equation: $\lg [In]/[Cd] = 0.639 + 0.448 \lg [OS-20]$. The author further concluded that the dependence of alloy composition on surfactant concentration in the case of other alloys may be described by the following general equation: $\lg [Ne_1]/[Me_2] = A + B \lg [surfactant]$. Further calculations made for the cases of Sn-Pb and Sn-Cu confirmed the validity of the two equations. References 4: Russian.

Composition of Cu-Ni Films Deposited on Substrate While Sputtered by Ar Ions

927D0159G Moscow FIZIKA I KHIMIYA OBRABOTKI MATERIALOV in Russian No 1, Jan-Feb 92 (manuscript received 13 Feb 91) pp 82-85
[Article by K.V. Kosterin, Ivanovo; UDC 621.793.182:621.793.71]

[Abstract] An experimental study of simultaneous deposition of Cu-Ni films on a substrate and their sputtering by Ar ions was made, the apparatus consisting of a Penning Ar-ion source in a longitudinal magnetic field with the anode between two cathodes. The experiment was performed with a target-cathode, made of 50 Cu-50 Ni alloy and with the target-cathode made of 99 Cu-1 Ni alloy. A titanium substrate was placed between the anode and the target-cathode, whereupon a bias voltage was applied to it (500 V for film deposition from the 50 Cu-50 Ni cathode, 80 V for film deposition from a 99 Cu-1 Ni cathode) while a voltage was applied to the both cathodes. The cathode voltage was varied over the 500 to 1000 V range. While a film was depositing on the substrate, it was being sputtered by ions, which the bias voltage had extracted from

the discharge plasma in the interelectrode space. This ion flux was nonhomogeneous, its density varying from zero at the periphery to a maximum at the axis of the ion source, but that maximum density was sufficiently high to locally sputter away the entire deposited material. The ratio of deposited atom flux to sputtered atom flux thus varied over the substrate surface and so did correspondingly the film thickness, from maximum at the periphery to zero at the axis. An X-ray microanalysis of the films across the substrate surface for Cu, Ni, and Ti content revealed a corresponding taper of the Cu content with an attendant Ni enrichment, to 100 percent Ni in films deposited from the 50 Cu-50 Ni target and to 70 percent Ni in films deposited from the 99 Cu-1 Ni target. The sum of Cu and Ni signals from was assumed to be proportional to the film thickness, such an assumption being valid for thin films with negligible signal self-absorption. The variation of Cu and Ni content cannot be explained by different sputtering rates of these metals, inasmuch as the partial Ni sputtering rate would have to be much lower (zero for 100 percent Ni content) than it actually is, but may be explained by preferential diffusion of interstitial atoms. Figures 2; references 4.

On Mechanism of Chromium-Based Diffusion Coat Formation on Steel

927D0163F Moscow ROSSIYSKAYA AKADEMIYA NAUK: SERIYA METALLY in Russian No 2, Mar-Apr 92 pp 209-215

[Article by V.N. Mikhaylin, B.N. Chertov, L.Ya. Ratgauz, A.Yu. Novikov, Zaporozhye and Moscow; UDC 621.785.5]

[Abstract] The use of diffusion surface alloying for hardening and protecting parts of various machines and devices and its efficiency in mobile mixtures, e.g., furnaces with rotary chambers, are discussed, and attention is focused on diffusion surface chrome-plating. The mechanism of the Cr coat formation on the surface of steel is investigated, and a mathematical model of the process is formulated using a number of assumptions, particularly that Cr₂₃C₆ and Cr₇C₃ carbide layers grow not inward but outward and are limited by the carbon diffusion from the base through earlier formed layers; that the carbon concentration on the sample surface affecting the carbide formation energy and carbon diffusion mobility is equal to 0.1 percent, etc. The model makes it possible adequately to describe the diffusion chrome-plating process. The experimental results are consistent with theoretical data; they demonstrate that within a 0.3 to 0.6 percent carbon concentration range in steel, the chromium solution layer in α -iron grows outward by 35 to 40 percent and inward by 60 to 65 percent which is also consistent with the experimental findings. An analysis of the total Cr concentration on carbide layer-based coats and areas of Cr solution in iron and steel with various carbon concentrations demonstrates that the greatest mass transfer flux is ensured at a 0.7 to 1.0 percent carbon concentration. Figures 2; tables 2; references 10: 8 Russian, 2 Western.

Gallium Interaction With Aluminum Films

927D0163G Moscow ROSSIYSKAYA AKADEMIYA
NAUK: SERIYA METALLY in Russian No 2,
Mar-Apr 92 pp 220-222

[Article by G.F. Ivin, Moscow; UDC 669.871-154+669.71]:536.777]

[Abstract] The interaction of liquid gallium with a thin layer of aluminum applied to a substrate is examined within a broad temperature range of 22 to 238°C, and the effect of the substrate material on the rate of this interaction is investigated. KDB-10 silicon wafers as well as silicon wafers with a vanadium and RSZ710 sublayers are used as the substrates; 1-2 μm thick aluminum films are applied by the thermal spraying method. The effect of the exposure duration on the radius of Ga penetration into the Al layer on pure silicon and silicon+sublayer substrates at various temperatures and the effect of the temperature at a one second exposure on the Ga penetration radius into the Al layer on pure silicon and silicon+sublayer substrates at various Ga sphere diameters are plotted; analytical formulas are derived to express the above relationships. X-ray microstructural analyses of the products of Ga interaction with Al show that an alloy of 20 percent Ga+80 percent Al which has good ductility properties is formed. Figures 2; tables 2; references 3: 1 Russian, 2 Western.

Plasma Coats From Zirconium Dioxide Powder Produced by Sol-Gel Technology

927D0164E Kiev POROSHKOVAYA
METALLURGIYA in Russian No 3 (351),
Mar 92 pp 38-41

[Article by I.N. Gorbato, A.Ye. Terentyev, O.M. Rozenal, A.I. Sesikov, Yu.D. Repkin, I.I. Timofeyeva, A.G. Khismatulin, L.A. Nadtochiy, Institute of Materials Science Problems at the Ukrainian Academy of Sciences, Kiev; UDC 621.791.927.55]

[Abstract] The advantages of refractory powder oxides with relatively large hollow particles with thin walls which ensures good flowability and sufficient particle heating in the plasma jet of commercial devices even in the case of plasma jet spraying of relatively low-melting compositions are summarized, and it is shown that plasma coats made from zirconium dioxide powders stabilized with magnesium, calcium, and yttrium oxides have the best heat insulation properties. The stringent requirements imposed

on the purity, porosity, granulometric composition, and flowability of plasma spraying powder can be met by the sol-gel technology of synthesizing ZrO_2 powders stabilized with Y_2O_3 . A microscopy study demonstrates that after passing through plasma, all particle surface defects are eliminated completely, i.e., the powder is spheroidized. Powder calcination treatment for improving the technological properties is described, the technological properties of stabilized zirconium oxide powder are summarized, the properties of coats from stabilized zirconium oxide powders are examined, and the phase composition of stabilized zirconium dioxide powders and coats jet-sprayed from them are summarized. X-ray phase analysis reveals both cubic and tetragonal zirconium oxide in the initial powder and the coat. The use of stabilized zirconium dioxide powder produced by the sol-gel technology may expand the range of heat insulating coat applications on parts of gas turbine and adiabatic engines. Figures 2; tables 3.

Aluminum Oxide Electric Insulation Plasma Coats for Radio Electronic Equipment Heat Sinks

927D0164F Kiev POROSHKOVAYA
METALLURGIYA in Russian No 3 (351),
Mar 92 pp 45-47

[Article by V.G. Zilberberg, A.M. Vyaltsev, N.I. Kirkun, V.I. Pavlenko, B.V. Glebovskiy, Institute of Materials Science Problems at the Ukrainian Academy of Sciences, Kiev; UDC 621.762:661.862:621.793:621.396.6]

[Abstract] The need for new materials which ensure stable operation of radio electronic equipment both under normal climatic conditions and at a high relative humidity is identified, and the possibility of using heat sinks with an aluminum oxide layer deposited by plasma spraying is investigated. The plasma jet-spraying condition is optimized using *a priori* data by the mathematical experiment design method. Prototypes of heat sinks are tested in order to optimize the coat thickness, and it is shown that coats with a 0.35 mm thick layer have the optimum breakdown voltage of 3.5 and 2.3 kV DC and 2.5 and 2.0 kV AC before and after moistening, respectively, and a heat conductivity of 80 W/m·K and a volume electric resistivity of $1.6 \cdot 10^{12} \Omega \cdot \text{cm}$. Heat conductivity test data on electric insulation materials and coats are summarized and compared to those of traditional materials. Metallic heat sinks with ceramic coats are recommended for use as insulating elements in semiconductor devices. Tables 1; references 1.

Conjugate Processes During the Electrolytic Dissolution of Metals and Alloys

927D0155A Moscow ZASHCHITA METALLOV
in Russian Vol 28 No 1, Jan-Feb 92 pp 48-52

[Abstract of article by V. Yu. Kondrashin, Voronezh State University; UDC 541.138]

[Abstract] The concept of conjugate reactions, or chemical induction, during electrolytic processes was applied to explain the selective and uniform dissolution of binary alloys as well as the anodic dissolution and corrosion of metals. It was found that the transfer of energy from one electrochemical process (primary) to another (secondary) explains the phase transformations of the positive component during the selective dissolution of homogenous alloys, the drop in the anodic potentials of uniformly dissolving alloys, pseudoselective dissolution, and the possibility of the autolysis or anodic dissolution of a metal in the presence of acidic oxidizing agents at lower than equilibrium potentials. An inductive electrochemical reaction can proceed under quasi-inversive conditions if a specific change is made in its potential and it thereby becomes a source of energy. Figures 2; references 12: 11 Russian, 1 Western.

Estimating the Stationary Corrosion Rate of Metals Under Atmospheric Conditions

927D0155B Moscow ZASHCHITA METALLOV
in Russian Vol 28 No 1, Jan-Feb 92 pp 61

[Abstract of article by Din Vu, The National Center for Scientific Study of the Socialist Republic of Vietnam, Institute of Tropical Technology, Hanoi; Institute of Physical Chemistry, USSR Academy of Sciences; UDC 620.193.2]

[Abstract] A mathematical function was developed to determine the stationary rate of atmospheric corrosion in metals and to evaluate and compare the corrosion resistance of different types of metals. The formula was developed using data from conventional corrosion tests published in a number of different studies. Regression analysis of the data was performed on an IBM PC XT/AT using off-the-shelf computer software. Figures 6; tables 5; references 16: 5 Russian, 11 Western.

Corrosion Behavior of Sintered Heterophase TiN-Cr and TiN-Ni Materials in Sulfuric Acid Solution

927D0155C Moscow ZASHCHITA METALLOV
in Russian Vol 28 No 1, Jan-Feb 92 pp 62-69

[Abstract of article by T. V. Chukalovskaya, N. D. Tomashov, and F. F. Yegorov, Institute of Physical Chemistry, USSR Academy of Sciences; UDC 620.193.4]

[Abstract] The corrosion behavior of sintered heterophase TiN-Cr and TiN-Ni materials was studied to determine the relationship between this behavior and the phase composition and structure of these materials and sintering time and temperature. Block-shaped specimens, 5 x 5 x 20 mm, were cold pressed from powders containing 5 to 60 percent chromium or nickel and sintered at 1650-1900°C for 90

minutes to two hours in an argon atmosphere. Corrosion tests were performed in a 0.5 M solution of sulfuric acid at room temperature (20-22°C). Total corrosion was estimated from loss of mass. The quantity of Ti passing into the solution during corrosion was estimated spectrophotometrically using dianthypyrimethane. These data were used to determine the overall corrosion rate and the rate at which Ti was dissolved out of the materials, as well as the coefficient of Ti dissolution, which is the ratio of Ti content in the solution to its content in the material. In theory, this coefficient should characterize the structural selectivity of corrosion for heterophase materials. The microstructure and phase composition of the sintered specimens were studied on a DRON-3 diffractometer in Cr and Ni radiation. It was found that complex heterophase structures are formed during sintering and that these structures consist of Ti nitrides and a complex metal matrix. As sintering time and temperature are increased, the proportion of metal in solid solution form decreases, and the composition of the Ti nitrides changes to where the proportion of TiN with Cr or Ni dissolved in it increases and the proportion of defective non-stereometric nitride decreases. TiN-Cr materials under the conditions described herein are quite passive and dissolve very slowly (0.001-0.01 g/(sq m/h)). In the TiN-Ni specimens, the nickel phases are in an active state that determines the structurally selective nature of the corrosion and the relatively high rates at which the material corrodes (0.1-1.5 g/(sq m/h)). As the concentration of the metal component is increased, the corrosion rate of TiN-Cr sharply drops, but increases in the case of TiN-Ni. The kinetics of the corrosion process are characterized by slower corrosion rates for TiN-Cr, and somewhat faster rates for TiN-Ni. As sintering time and temperature are increased, the corrosion resistance of both materials increases. Figures 3; tables 3; references 17: Russian.

Corrosion Behavior of Chromized Steel 45 in Sulfuric and Hydrochloric Acid Solutions

927D0155D Moscow ZASHCHITA METALLOV
in Russian Vol 28 No 1, Jan-Feb 92 pp 70-76

[Abstract of article by S. G. Babich, V. M. Knyazheva, I. I. Zayets, Yu. Ye. Roginskaya, L. Ye. Alekseyenko, and Ye. F. Koloskova, Scientific Research Institute of Physics and Chemistry imeni L. Ya. Karpov; UDC 620.193.2]

[Abstract] The corrosion resistance of chromized steel 45 to sulfuric and hydrochloric acid solutions was studied. Specimens 20 mm in diameter and five mm thick were degreased with ethanol and rinsed twice with distilled water. Electrochemical measurements were carried out in a cell constructed so that solution samples could be taken without destroying specimen polarization. Solution samples were analyzed using the atomic adsorption method with the aid of a Perkin-Elmer 503 spectrometer. The phase composition of the coatings was studied on a DRON-3 diffractometer. Auger electron spectroscopy performed on a Varian spectrometer was used to find the elemental composition of the coatings. It was found that the external layer of steel 45 chromized and borochromized in atmospheric air consists primarily of

$\text{Cr}_2\text{C}_x\text{N}_y$ -type chromium carbonitride. Chromizing steel 45 increases its corrosion resistance by two to three orders of magnitude over a wide range of potentials in both sulfuric and hydrochloric acids, and borochromizing increases its corrosion yet another two to three-fold. Successful long-term utilization of chromized and borochromized carbon steels in acidic reducing media is complicated by substrate dissolution through coating microdefects. The influence of the latter is substantially reduced when potentials are within the range of 0.6-1.05 V, where substrate passivation becomes possible. Corrosion resistance can be substantially enhanced by changing coating composition from chromium carbonitrides to chromium carbides. Figures 3; tables 1; references 12: 10 Russian, 2 Western.

Corrosion of Ferrous Metals in Solutions of Zinc Bromide and Calcium Bromide

927D0155F Moscow ZASHCHITA METALLOV
in Russian Vol 28 No 1, Jan-Feb 92 pp 129-131

[Abstract of article by V. N. Gnusin, V. A. Mosin, and T. Ye. Rozhova, All-Union Scientific Research Institute of Petroleum Engineering, Krasnodar; UDC 622.276.5.05:620.193]

[Abstract] The corrosion mechanism of ferrous metals in zinc and calcium bromide solutions was investigated. A P5827M potentiostat was used to record polarization curves from a stationary disk electrodes made of steel 30, referenced to a saturated silver chloride electrode. The tests were performed in a thermostatically controlled electrolytic cell containing a saturated aqueous salt solution of 22 percent ZnBr_2 plus 51 percent CaBr_2 , a weakly diluted solution of 21 percent ZnBr_2 plus 49 percent ZnBr_2 , or solutions containing from 20 to 80 percent ZnBr_2 . Stable hydrodynamic conditions were maintained by a magnetic agitator with a controlled speed of rotation. The solutions were deoxidized by blowing helium through them for 30 minutes, with oxygen content measured by a K-215 oxymeter. Weight measurements were taken in accordance with State Standard 9.502-82. The test results, which were compared with those for other types of ferrous metals (steel 40G, SM90SSI from Japan, and CSh-18 cast iron) showed that long-term immersion of steel articles in saturated zinc bromide solutions leads to surface passivation and reduces the corrosion rate to 0.1 mm/year and less. Oxygen and the rate of agitation have little effect in these solutions. Dilution and elevated temperatures increase the rate of corrosion. Corrosion failure is accelerated by processes such as erosion and friction, which damage the surface layer of the metal. In view of the fact that fluids based on zinc bromide compositions are widely used through the petroleum industry, and under extremely harsh conditions, further research in this area is essential. Figures 3; tables 1; references 3: 1 Russian, 2 Western.

Effect of Pre-Carburization on the Anti-Corrosion Properties of Chromized Low-Carbon Steel

927D0155G Moscow ZASHCHITA METALLOV
in Russian Vol 28 No 1, Jan-Feb 92 pp 140-143

[Abstract of article by I. S. Litmanovich and Ya. M. Zolotovitskiy, Temp Scientific Production Association,

Moscow, and Technopribor Special Technical Design Bureau, Gomel; UDC 620.193.2]

[Abstract] The feasibility of applying corrosion-resistant chromium carbide coatings to pre-carburized low-carbon steel was investigated. Two types of 10kp steel specimens were used: cylinders eight mm in diameter with a surface area of one sq cm for testing electrochemical corrosion characteristics, and plates 4 x 30 x 40 mm for corrosion tests in a moisture chamber. Specimens were powder carburized by sprinkling them with charcoal, placing them in a covered steel container, and heating them for two hours at 900 to 1200°, depending on the degree of carburization desired. Carburized and uncarburized specimens were chromized by placing them in a steel container, sprinkling them with a chromizing mixture (50 percent FKh100A ferrochromium, 45 percent alumina, 5 percent ammonium chloride), and heating them for four hours at 1150° in a protective RX gas atmosphere to obtain a coating 30 to 40 µm thick. Corrosion resistance was cyclically tested in a moisture chamber by first exposing the specimens for eight hours to a temperature of 55 ± 2° and a humidity of 95 ± 3 percent and then exposing the specimens to 100 percent humidity for 16 hours while allowing the chamber to gradually cool from 55 to 20°. This 24-hour cycle was repeated 10 times, with corrosion resistance evaluated from the amount of time that passed between the end of the test and the onset of corrosion and loss of specimen mass. Electrochemical corrosion characteristics were measured by recording polarization curves with the aid of a PI-50-1 potentiostat and an LKD4-003 plotting device after immersing the specimens in corrosive solution for 16 hours. A chromium carbide coating highly resistant to corrosion in humid conditions can be applied to low-carbon steel parts by carburizing the steel at 1100 to 1150° for two hours, chromizing it at 1150° for four hours, and chemically passivating it in an aqueous solution of potassium bichromate. Tables 1; references 4: Russian.

Corrosion of Steel and Nickel Steel Alloys in Nitrosylchloride

927D0155H Moscow ZASHCHITA METALLOV
in Russian Vol 28 No 1, Jan-Feb 92 pp 143-146

[Abstract of article by B. A. Gru, A. I. Tsinman, and E. E. Pfefer; UDC 620.197]

[Abstract] The corrosion behavior of steel and nickel steel alloys in media containing nitrosylchloride were studied. The NOCl used in the study was synthesized from KCl and liquid N_2O_4 made by double distilling process nitrogen oxides. The NOCl, the purity of which was controlled by means of UV and IR spectra, boiling temperature (-5.8°), and crystallization temperature (-61.5°), contained no less than 99.8 percent nitrogen oxide. Corrosion tests were carried out using mixtures consisting of 15 percent NOCl + 37 percent Cl_2 + 48 percent N_2O_4 , which are identical to actual process gas mixtures subject to rectification, pure NOCl, NOCl mixed with nitrogen oxide or chloride, and humidified mixtures. Weight tests were performed in glass ampules which, together with their specimen content, were cooled with dry ice to -10 to -20°, doused in one of the

corrosive mixtures, and sealed. The specimens were tested at room temperature. Potentiometric curves were taken by a P-5827 M potentiostat in one V/hr intervals in 50 mV increments and were supplemented by measurements of lost electrodes mass. In the ternary mixture, the nickel-chromium and nickel-chromium-molybdenum steels corroded at a rate of 5 to 15 g/(sq m/h), while the alloys containing more than 50 percent nickel were corrosion-resistant. Pure NOCl reacts aggressively with steel, but does not attack high-nickel alloys, although the corrosion potentials for both metals are nearly the same. The corrosion resistance of nickel and its alloys decreased in highly humidified NOCl, but chromium, molybdenum, and tungsten increased the corrosion resistance of the test alloys in this medium. The addition of chloride to NOCl results in lower corrosion potentials and the complete passivation of high-nickel alloys. Steel and nickel alloy corrosion resistance can also be increased by adding nitrogen dioxide to the NOCl. Thus, high-nickel alloys are recommended for the fabrication of vessels designed to contain NOCl media. Figures 2; tables 2; references 17: 13 Russian, 4 Western.

The Electrochemical and Corrosion Behavior of Nickel in Sulfuric Acid Solutions

927D0156A Moscow ZASHCHITA METALLOV
in Russian Vol 28, No 2, Mar-Apr 92 (manuscript
received 22 Apr 91) pp 191-195

[Article by A.E. Kozachinskiy, A.P. Pchel'nikov, Ya.B. Skuratnik, and V.V. Losev, Physics and Chemistry Scientific Research Institute imeni L.Ya. Karpov; UDC 620.193.41/546.74]

[Abstract] The authors of the study reported herein examined the corrosion and electrochemical behavior of nickel in sulfuric acid solutions. The studies were performed in a deaerated solution of 1 N H₂SO₄ at 20°. Electrochemical and corrosion radiochemical measurements were taken in order to simultaneously determine the partial rates of the dissolution of the nickel and the ionization of its interstitial hydrogen. Before the experiment, the specimen was subjected to electropolishing in a solution of 60 percent H₂SO₄ at $i = A/cm^2$ to remove its surface oxides and create a reproducible electrode surface. Next, the specimen was rinsed in bidistillate, dried with filter paper, suspended for 30 minutes in a cell over a solution in an argon atmosphere, and then dropped into the solution. The experiment established that hydrogen entering the nickel during the corrosion process reduces the speed at which the nickel corrodes and also slows anodic dissolution. This effect of hydrogen is attributed to the fact that during the corrosion process, hydrogen is gradually absorbed by the nickel atoms located in the polycrystalline positions ("active centers"), and just like preliminary cathodic polarization, this leads to a reduction in the nickel's anodic activity. The adsorbed hydrogen is partially transformed into an absorbed state, thus diffusing into the depths of the metal and partially moving from the surface in molecular form. The effect of cationic-type corrosion inhibitors on the corrosion and hydrogen absorption of nickel was also examined by way of the example of the corrosion inhibitor KI-1. The experiment performed confirmed that KI-1

reduces both the rates of corrosion and hydrogen absorption. The authors concluded by stating that because of the changes in the electrochemical behavior of nickel that occur during the corrosion process, information about corrosion-related losses of nickel may only be obtained by using direct methods of analyzing solutions. Figures 3; references 7: 6 Russian, 1 Western.

The Corrosion and Electrochemical Behavior of Aluminum-Iron-Nickel Bronze in a Chloride Solution

927D0156B Moscow ZASHCHITA METALLOV
in Russian Vol 28 No 2, Mar-Apr 92 (manuscript
received 24 Jan 91) pp 196-200

[Article by V.N. Chervyakov, L.V. Kharkova, B.P. Aravin, and A.P. Pchel'nikov, Physics and Chemistry Institute imeni L.Ya. Karpov and Prometey Central Scientific Research Institute of Construction Materials; UDC 620.193/669.35.6]

[Abstract] The authors of the study reported herein examined the corrosion and electrochemical behavior of AZh-NMts aluminum-iron-nickel bronze in a chloride solution. The study specimens were cast and annealed at 900° for one hour and then tempered for one hour at 600° (mode one) or else at 350° (mode two). Before the tests, the specimens were cleaned with emery paper and degreased with ethanol. The corrosion tests were performed at 80° for five and 2,000 hours. After 2,000 hours had elapsed, polished sections of the specimens were prepared for metallographic studies. Their corrosion was studied in aerated solutions of 0.5 N NaCl + 0.03 N HCl in artificial sea water. The electrochemical measurements were conducted in deaerated solutions of 0.5 N NaCl + 0.03 N HCl and 0.5 N NaCl. The electrolyte was acidified to facilitate total passage of the corrosion products into the solution. The solution was analyzed by atomic adsorption chromatography (on Al and Mn) and by radiometry (on Cu, Fe, and Ni²⁺). The studies performed demonstrated that one hour of annealing at 900° followed by tempering for one hour at 600° reduces the susceptibility of aluminum-iron-nickel bronze to pitting corrosion by facilitating the selective dissolution and elimination of rich iron phases from the cast bronze. Figures 4; tables 2; references 13: 7 Russian, 6 Western.

The Impedance of a Corroding Titanium Electrode in Acid Solutions

927D0156C Moscow ZASHCHITA METALLOV
in Russian Vol 28 No 2, Mar-Apr 92 (manuscript
received 11 Mar 90) pp 202-209

[Article by Kh.G. Kuchukbayev, V.I. Kichigin, and L.V. Kondakova, Natural Science Institute, Perm State University; UDC 620.193:537.311.6]

[Abstract] The authors of the study reported herein measured the impedance of a corroding titanium electrode in solutions of 1 to 14 M H₂SO₄ and 2 to 6 M HCl. The measurements were taken in the frequency range from 10⁵ to 10⁻³ Hz depending on the surface pretreatment regimen and deaeration of the solution. Cylindrical specimens of

type VT1-0 and VT1-000 technical-grade titanium measuring 2 to 4.5 mm in diameter and pressed into Teflon were studied. The working surface of each specimen was in the form of a torus. Four different methods of treating the electrode surfaces of different specimens were used: treatment with emery paper with a grain size of 50 μm , M10 emery paper, ASM 20/14 NOM diamond paste, or else electrochemical polishing in a mixture of $\text{CH}_3\text{COOH} + \text{HClO}_4$. The measurements were taken at room temperature. The hodographs of the impedance of a corroding titanium electrode in aerated H_2SO_4 solutions were found to represent two well-demarcated semicircles in the capacitive half-plane. As the concentration of the H_2SO_4 solution was increased, the ratio of the diameter of the first (high-frequency) semicircle to the diameter of the second semicircle increased. The centers of the semicircles were located somewhat below the real axis. The extent of the center's shift was characterized by the angle ϕ between the abscissa and radius passed to the point where the semicircle intersects the axis of the abscissa. In the case of electrodes with a roughly treated surface, $\phi = 13$ to 15° for the high-frequency arc in 20 percent H_2SO_4 . As the concentration of H_2SO_4 increased, ϕ decreased in both the first and second semicircles. When the H_2SO_4 concentration was below 40 percent, the value of ϕ decreased by 5 to 7° for electrodes with a smoother surface (i.e., those polished with the M10 emery paper). When such was the case, the center of the low-frequency semicircle was located on the real axis. At higher H_2SO_4 concentrations, however, the very same surface treatment technique had little effect on the position of the semicircles' centers. For the electropolished and diamond paste-treated surfaces, moreover, ϕ actually increased ($\phi = 25$ to 30° for the high-frequency semicircle in 20 percent H_2SO_4). On the other hand, it was established that deaerating the H_2SO_4 solution with hydrogen resulted in a decrease in ϕ regardless of the surface treatment method used even though it did not have any marked effect on the polarization resistance or the ratio of the diameters of the two semicircles. When the H_2SO_4 concentration was above 70 percent, a third arc appeared on the hodograph. The researchers obtained a satisfactory agreement between the calculated hodographs and experimental data for the case of a four-step anodic mechanism that they have proposed. The said mechanism differs from the mechanism of anodic dissolution of titanium proposed elsewhere only in that the mechanism proposed herein considers only the active region of the process. On the basis of the studies performed, the authors concluded that the technique of measuring impedance permits a sufficiently precise and accurate determination of the rate at which a titanium electrode is corroding and a method for studying the kinetics of the corrosion destruction of titanium in acid media. Figures 4; table 1; references 25: 7 Russian, 18 Western.

The Effect of Lithium Additives on the Corrosion Properties of Aluminum

927D0156D Moscow ZASHCHITA METALLOV
in Russian Vol 28 No 2, Mar-Apr 92 (manuscript
received 19 Feb 91) pp 210-217

[Article by V.S. Sinyavskiy, A.M. Semenov, and V.D. Valkov, VILS Scientific Production Association; UDC 620.193./546.621]

[Abstract] The authors of the study reported herein examined the effect of lithium additives on the corrosion properties of aluminum. Pressed bands, measuring 10 x 100 mm, of three lithium-aluminum alloys containing 0.8, 1.9, and 2.3 percent (by mass) lithium, respectively, were used for the experiments. All of the study alloys also contained 0.1 percent zirconium. Type A995 pure aluminum was used for comparison. Tests for resistance to stratifying corrosion, intercrystallite corrosion, total corrosion based on mass loss, and corrosion cracking were conducted in accordance with the applicable all-union state standards [GOST]. The electrochemical characteristics of the study specimens were determined from polarization diagrams plotted by using a PI-50-1 potentiostat in a 0.5 M solution of NaCl. A Neophot-2 microscope and JEM-100CX transmission electron microscope were used for the metallographic studies, and the atmospheric tests were conducted on stands on the Izumrud scientific-research vessel in a tropical sea atmosphere for one year. The tests performed established that all of the study alloys, whether artificially aged to maximum strength or not, have high resistances to all of the aforesaid types of corrosion thanks to the absence of any electrochemical nonuniformity of their body and grain boundaries. An interconnection was established between the lithium content in the aluminum alloys and their rates of corrosion-induced mass loss. For the alloy consisting of aluminum and 0.8 percent Li, the rate of mass loss was higher than that for pure aluminum by a factor of 30. As the lithium concentration was increased to values exceeding its solubility in aluminum (1.3 percent), the rate at which the aluminum-lithium alloys (i.e., Al-1.9 percent Li and Al-2.3 percent Li) corrode was no longer dependent on the amount of lithium in the alloy. This was attributed to anodic dissolution of the $\delta'(\text{Al}_3\text{Li})$ phase, which provides electrochemical protection for the matrix. The electrochemical characteristics of the study alloys were determined as a function of their lithium content and artificial aging mode. When up to 2.3 percent lithium was added, more negative potentials were established to the following extents: by 0.149 V for corrosion; by 0.053 V for pitting formation; and by 0.065 V for repassivation. When the duration of artificial aging was increased to 144 hours, all of these electrochemical characteristics were shifted virtually identically in a negative direction. Figures 5; tables 4; references 8: 5 Russian, 3 Western.

The Effect of Diamond Smoothing on the Resistance of Cr17Ni15 Steel to Chloride Corrosion Cracking

927D0156E Moscow ZASHCHITA METALLOV
in Russian Vol 28 No 2, Mar-Apr 92 (manuscript
received 30 Aug 90) pp 218-222

[Article by V.S. Kropachev, V.P. Pogodin, L.A. Khvorostukhin, and V.A. Gashenko, All-Union Scientific Research Institute of Inorganic Materials imeni A.A. Bochvar; UDC 620.194]

[Abstract] The authors of the study reported herein examined the effect of diamond smoothing on the resistance of Cr17Ni15 steel to chloride corrosion cracking. Plane (80 x

5 x 0.5 mm), annular (6 x 5 x 0.3 mm), and tubular ($\phi = 12.55$ mm, length = 100 to 120 mm, thickness = 0.3 mm) specimens of austenite (1,050°, 30 minutes) Cr17Ni15 steel were subjected to preliminary electropolishing in a solution of $H_3PO_4 + CrO_3$. The plane specimens were mechanically deformed 15 percent by rolling on a laboratory mill, and the tubular specimens were deformed by drawing on a KhPTR mill. The plane specimens were bent into rings on a cylindrical mandrel, and their ends were secured in holders. This was done to create the tensile stresses required during the corrosion cracking tests. The annular specimens were loaded by squeezing them into a cylinder of the very same material with a diameter 10 percent larger than the inner diameter of the specimens. The tubular specimens were loaded with argon pressure from the inside. Diamond smoothing was performed on shaving (in the case of the plane specimens) or turning (in the case of the tubular and annular specimens) mills. The following were varied: diamond radius, number of spindle rotations, tool feed rate, and force used to press the diamond to the surface being worked (i.e., smoothing force). Tests performed on the specimens after the various modes of smoothing established that diamond smoothing with a force of less than 100 N may indeed be used to work the surfaces of thin-walled (≤ 0.5 mm) products made of Cr17Ni15 steel so as to increase their resistance to chloride corrosion cracking in aqueous media provided that the loads on the metal are below their tentative yield point ($\sigma < \sigma_{0.2}$). When the said products are more highly loaded, diamond smoothing is not feasible. The effectiveness of diamond smoothing in increasing the chloride corrosion cracking resistance of Cr17Ni15 steel was attributed to the residual compressive stresses formed in the surface layer of the steel products during the diamond smoothing process. Figures 2; tables 3; references 7 (Russian).

Determining the Tendency of 14Cr17Ni2 Steel to Intercrystallite Corrosion by an Accelerated Electrochemical Method

927D0156F Moscow ZASHCHITA METALLOV
in Russian Vol 28 No 2, Mar-Apr 92 (manuscript received 18 Sep 90) pp 223-226

[Article by N.D. Tomashov, G.P. Chernova, G.K. Radetskaya, Ye.A. Nasedkina, M.T. Osokina, and O.G. Yermolina, Physical Chemistry Institute, USSR Academy of Sciences; UDC 620.196]

[Abstract] The authors of the study reported herein developed an accelerated electrochemical method of determining the tendency of 14Cr17Ni2 steel toward intercrystallite corrosion. They based their development effort on the existing method of determining the tendency of austenite-class stainless steels (Cr18Ni10Ti, 12Cr17Mn9Ni4, etc.) toward intercrystallite corrosion based on corrosion potential or the taking of anodic curves in a solution of 5 percent $HNO_3 + 20$ g/l $FeCl_3 \cdot 6H_2O + n$ ml/l HCl (with the amount of HCl depending on the specific type of steel). The studies performed confirmed that the tendency of 14Cr17Ni2 steel toward intercrystallite corrosion may be qualitatively determined based on its type of anodic polarization curve (i.e., by the presence of a

second maximum in the polarization curve) and may be semiquantitatively determined based on the maximum anodic current when $E_c = +0.15$ V. The drop method and the technique of taking polarization curves under laboratory conditions was used to test 50 specimens (30 with no tendency toward intercrystallite corrosion and 20 with a tendency toward intercrystallite corrosion) in a solution of 5 percent $HNO_3 + 20$ g/l $FeCl_3 \cdot 6H_2O + 30$ ml/l HCl. An additional 196 specimens were tested under commercial conditions. The results obtained by the proposed acceleration method and those of standard tests performed in accordance with All-Union State Standard [GOST] 6032-84 were found to be in agreement with one another to a level of 95 percent. Figures 4; table 1; references 5: Russian.

Measuring the Initial Rate of the Corrosion of Steel in High-Purity Water

927D0156G Moscow ZASHCHITA METALLOV
in Russian Vol 28 No 2, Mar-Apr 92 (manuscript received 4 Apr 89; after revision 4 Jun 91) pp 227-230

[Article by L.N. Moskvina, A.A. Yefimov, Ye.Yu. Khari-tonova, V.F. Teterin, and V.I. Toftul, Technology Scientific Research Institute; UDC 620.193/546.212]

[Abstract] Procedures have previously been described for measuring the rates at which steels corrode in electrolyte solutions by using the radioisotope ^{59}Fe ($T_{1/2} = 45.6$ days) created by activating the metal with thermal neutrons. The absorbed dose must not exceed 300 to 500 krad (the integral flux must not exceed 10^{19} neutrons/cm²) so as not to cause deep and irreversible changes in matrix structure. In practice, the peak at 1,099.3 keV is used for quantitative determination of ^{59}Fe on a Ge(Li) detector. When a specimen is irradiated with an integral flux of 8×10^{18} neutrons/cm², the detection threshold of iron by γ -spectrometry based on ^{59}Fe on a type DGDK-50B detector amounts to 8.6×10^{-9} g in a specimen that has been exposed for 100 hours during the spectrometric measurement process. In electrolyte solutions, iron concentrations surpassing the detection threshold and sufficient for reliable measurement of γ -spectra are achieved after one to three minutes. In high-purity (i.e., deeply demineralized) water, the detection threshold is only exceeded after 0.25 to 1.0 hours at room temperature under static conditions. In the initial stages of contact, the time dependence of the concentration of the tracer radionuclide passing into the water is linear. The authors of the study reported herein have used this fact as a basis for developing a method of measuring the initial rate of the corrosion of steel in high-purity water by radiometric determination of the rates of entrainment of tracer radionuclides into the water. They have described a method for making such estimates by way of the example of the type 20 steel in highly demineralized water at temperatures ranging from 20 to 100°C. ^{55}Fe and ^{59}Fe were both used as tracer isotopes. The proposed method may be used for a one-time determination of the rate at which steels corrode in their initial stages of contact with demineralized water, as well as to study the change in corrosion rates over time. The rate of corrosion (K , g/(m² x h)) of test specimens was estimated

in accordance with the formula $K = m_0 A_t e^{(0.693t/T) 1/2}$ $V_s/\tau S$, where m_0 is the calibrated coefficient of the transition from units of the tracer isotope's activity to the units of the total iron concentration in g/dm^3 ; t is the time from the moment when m_0 was determined to the moment when the sample of the solution was measured in hours; A_t is the specific activity of the tracer isotope at the moment in time t in the sample of solution in contact with the test specimen in Becquerels/ dm^3 ; $T_{1/2}$ is the tracer isotope's half-decay period in hours; S is the contact area of the demineralized water with the test specimen in m^2 ; and V_s is the volume of the measured sample of the solution of the tracer radionuclide in dm^3 . Figures 2; references 11: 10 Russian, 1 Western.

The Composition of the Surface of Corroded Ti-W Alloys

927D0156H Moscow ZASHCHITA METALLOV
in Russian Vol 28 No 2, Mar-Apr 92 (manuscript
received 19 Mar 91) pp 295-297

[Article by I.V. Kasatkina, R.Kh. Zalavutdinov, A.I. Shcherbakov, Physical Chemistry Institute, USSR Academy of Sciences; UDC 620.193.01]

[Abstract] The authors of this concise report used the technique of X-ray spectral microanalysis to study the effects of corrosion on the surface of titanium-tungsten alloys. The study alloys contained 0.7, 2.2, 3.8, and 9.3 percent tungsten, respectively. The test specimens were placed in 2.5 M H_2SO_4 . The distribution of tungsten in the surfaces of polished and etched specimens was studied. The tungsten concentration on the surfaces of the alloys containing 0.7 and 2.2 percent tungsten was found to be weakly dependent on exposure time. The alloys with the higher tungsten contents were found to undergo an increase in the intensity of tungsten on their surfaces after only small test periods (up to one hour). As the holding times were increased, the rate of tungsten accumulation decreased; the lower the concentration of tungsten in the alloy, the earlier this decrease occurred. The data confirmed that the lower the alloy's tungsten content, the more quickly a stationary concentration of tungsten in the alloy's surface layer is established. The outer portion of the tungsten-enriched layer was easily separated. The study results also led the authors to hypothesize that when the amount of tungsten in an alloy is small, the surface diffusion redistribution of tungsten required for formation of an inherent tungsten phase does not have time to occur. According to the study data, the rate of the alloys' dissolution in the interval from 30 to 70° changes by about two orders of magnitude, whereas the intensity of radiation changes only by a factor of about two. In other words, the accumulation of tungsten on the alloy's surface is in fact not determined by the rate of dissolution, but instead depends solely on the starting content of tungsten in the alloy. These results confirmed the hypothesis that a definite degree of tungsten surface enrichment is required for individual alloy compositions. As the exposure time and corrosiveness of the test media were increased, the fraction of effectively functioning tungsten decreased. Figures 2; tables 2; references 3: 2 Russian, 1 Western.

The Effect of High-Temperature Thermomechanical Treatment on the Corrosion Cracking of Carbon Austenite Steel

927D0156I Moscow ZASHCHITA METALLOV
in Russian Vol 28 No 2, Mar-Apr 92 (manuscript
received 15 Jul 90) pp 303-306

[Article by Yu.N. Goykhenberg, M.A. Smirnov, and V.Yu. Vnukov, Chelyabinsk Polytechnic Institute; UDC 620.193]

[Abstract] The authors of this concise report examined the effect of high-temperature thermomechanical treatment on the corrosion cracking of type 50Cr4Mn18 austenite carbon steel. Blanks of 50Cr4Mn18 steel measuring 18 x 18 mm were heated to 1,050° and then subjected to intermediate cooling to 1,000° and five minutes of holding. They were deformed 30 percent by rolling and reduction and then quick-cooled in water so as to prevent the development of recrystallization processes and to form a toothed pattern in the grain boundaries and a developed structure in the grain bodies. Some of the blanks were tempered directly in water while their temperature was still 1,050°. The blanks that were tempered directly after high-temperature thermomechanical treatment experienced an increase in yield point from 405 to 530 and an increase in ultimate strength from 970 to 1,060 MPa along with a slight decrease in relative elongation (from 74 to 62 percent). Corrosion cracking tests performed directly after the tempering and high-temperature thermomechanical treatment at stresses of 350 and 470 MPa, respectively, did not result in any specimens breaking over the 4,000-hour test period, even though traces of overall corrosion had already appeared. Blanks of 50Cr4Mn18 steel are used to make turbogenerator shrink rings; they undergo finishing cold or warm workhardening to $\sigma_{0.2} = 900$ to 1,150 MPa. In view of this fact, some of the study blanks were hardened by cold straining with different degrees of deformation following tempering or high-temperature thermomechanical treatment. This stretching was performed at 900 to 1,500 MPa. The beneficial effects of high-temperature thermomechanical treatment from the standpoint of making steel more resistant to corrosion cracking were very evident during the tests performed on the specimens that had been exposed to the additional cold straining: Their time to fracture increased by a factor of 1.7 to 3. Aging reduced the corrosion cracking resistance of the specimens subjected to high-temperature thermomechanical treatment. This decrease was far smaller than in the case of the absence of any thermomechanical treatment, however. The time to fracture of those specimens that had been aged after high-temperature thermomechanical treatment was about the same as that of the specimens that were tempered but not aged. The studies performed thus confirmed that when applied to austenite steel with a high carbon content, the technique of combining high-temperature thermomechanical treatment and additional cold straining provides better protection against corrosion cracking than does tempering followed by deformation to the same strength level. This finding was attributed to the fact that intercrystallite destruction becomes more difficult. Aging, which leads to a catastrophic decrease in the

durability of tempered steel, does not have as detrimental an effect after high-temperature thermomechanical treatment, which reduces the localization of embrittling carbide phases. Figures 2; references 9: Russian.

The Effect of HCl and Molasses on the Corrosion of 12Cr18Ni10Ti Steel in Phosphoric Acid Solutions

927D0156J Moscow ZASHCHITA METALLOV
in Russian Vol 28 No 2, Mar-Apr 92 (manuscript
received 4 Jun 90) pp 308-312

[Article by D.Kh. Kopeliovich and V.I. Ivlev, Mayak Production Association, Chelyabinsk; UDC 620.193.41]

[Abstract] In the process of solidifying radiochemical wastes into phosphate glass, phosphoric acid is used as the flux, and molasses is used as the reducing agent. The experience gained in using a mixture of 75 percent warm H_3PO_4 and molasses has demonstrated that this medium causes marked corrosion of equipment made of 12Cr18Ni10Ti steel. Because this corrosion is highly undesirable from the standpoint of both the integrity of the equipment and contamination of the acid with iron (which complicates the vitrification process), the authors of this concise report conducted a study to determine the possible causes for the increased corrosivity of a mixture of H_3PO_4 and molasses. The studies performed revealed that although the risk of corrosion of 12Cr18Ni10Ti steel in H_3PO_4 does increase when molasses is added to the H_3PO_4 , the H_3PO_4 causes 12Cr18Ni10Ti steel to corrode in and of itself even when not mixed with molasses. Consequently, refraining from the practice of adding molasses to phosphoric acid when encasing radiochemical wastes in glass will not completely resolve the corrosion problem. The authors have suggested that reliable protection against corrosion may be achieved by shifting the potential to the passive region. The conditions for anodic protection are, according to the authors, very favorable in unheated solutions containing no more than 1 g/l HCl when the width of the passive region is close to 1 V. They further state that the current density also drops sharply over time in a solution of 75 percent H_3PO_4 + 0.3 g/l HCl at 40° ($\epsilon = 0.4$ to 0.7 V) and is reduced to 10^{-2} A/m² after 15 to 30 minutes. Under these same conditions, a stable

passive state may be achieved by adding 1 to 3 g/l HNO_3 . Figures 2; tables 2; references 10: 8 Russian, 2 Western.

Corrosion of Aluminum and the Alloy TsAM4-1 in a Nickel Plating Electrolyte

927D0156K Moscow ZASHCHITA METALLOV
in Russian Vol 28 No 2, Mar-Apr 92 (manuscript
received 25 Jul 90) pp 321-322

[Article by V.P. Artamonov; UDC 620.193]

[Abstract] The alloy TsAM4-1 (Zn + 4 percent Al + 1 percent Cu) is widely used in machine building to manufacture components by means of precision casting. Such components are generally nickel-plated on a copper substrate precipitated from toxic cyanide electrolytes. When direct (i.e., without a copper substrate) nickel plating is used, the alloy dissolves in the electrolyte. In view of this fact, the author of this concise report studied the corrosion of aluminum and TsAM4-1 in a nickel plating electrolyte. Specifically, he studied the corrosion of A85 aluminum and TsAM4-1 in a nickel plating electrolyte containing the following (g/l): nickel sulfate, 250; nickel chloride, 50; boric acid, 40; saccharin, 2; and 1,4-butene diol, 0.2. A temperature of 50° and a pH of 4 were used. A Simultex unit was used for X-ray spectral analysis. The steps followed during the study were in accordance with a procedure detailed elsewhere. The studies performed revealed that TsAM4-1 consists of a β -phase (pure Zn), an α -phase (a solid solution of Zn in Al), an ϵ -phase ($CuZn_3$), and a eutectic of the specified phases. X-ray spectral analysis has shown that when TsAM4-1 is held in a nickel plating electrolyte for 0.5 to 16 hours, the electrolyte becomes enriched in nickel ions while the concentration of Al and Cu remain at the background level. The anodic corrosion process that occurs is obviously due solely to the dissolution of the zinc component of the TsAM4-1, and the aluminum and copper components are the cathode sections of its corroding surface. Although TsAM4-1 contains only four percent aluminum, its corrosion potential and time curves and its hydrogen and nickel evolution curves are closer to those of aluminum than zinc. TsAM4-1 corrodes much more slowly than zinc does. Depolarization of the cathodes occurs primarily as a result of the discharge of nickel ions, and less hydrogen is evolved. Figures 2; references 4: Russian.

Thermodynamic Analysis of Processes Occurring During Molten Steel Pool Blasting With Gas-Oxygen Jet

927D0152B Moscow IZVESTIYA VYSSHIKH UCHEBNIKH ZAVEDENIY: CHERNAYA METALLURGIYA in Russian No 1, Jan 92 pp 4-6

[Article by T.G. Sabirzyanov, N.I. Globa, B.A. Dvoryadkin, A.V. Petrov, Kirovograd Agricultural Machinery Institute and Kommunar'sk Integrated Iron and Steel Works; UDC 669.02/09:536]

[Abstract] A thermodynamic and thermal analyses procedure which makes it possible to find the expected equilibrium composition of the fuel combustion products at various temperatures and different oxygen rate coefficients α in oxygen-gas furnace tuyeres for steel smelting pools, to determine whether the incomplete fuel combustion products serve as reducing agents relative to the slag's ferrous oxide, and to establish whether the steel melting pool may be heated with the help of the incomplete fuel combustion products is proposed. The number of component moles produced by incomplete combustion of one mole of CH_4 , partial pressures of the components and CH_4 combustion products at various temperatures and α , and free energy of the $2(\text{FeO}) + \text{CO} + \text{H}_2 = 2\text{Fe}_{\text{liq}} + \text{CO}_2 + \text{H}_2\text{O}$ reaction at various temperatures are summarized. Tables 4; references 6.

Characteristic Features of Hydrodynamic Processes During the Pulsation Treatment of Metal in a Casting Ladle

927D0158B Moscow ROSSIYSKAYA AKADEMIYA NAUK: SERIYA METALLY in Russian No 1, Jan-Feb 92 (manuscript received 31 Jul 90) pp 13-19

[Article by Yu.I. Shish, L.V. Rubin, and A.D. Zrazhevskiy, Dneprodzerzhinsk; UDC 669.18.046.5]

[Abstract] The authors of the study reported herein used cold physical models to study the hydrodynamic processes occurring in a casting ladle during pulsation treatment of metal by setting it into a reciprocating motion in a submersible short tube by periodically changing the pressure in it while simultaneously adding various reagents and neutral gas through the tube. The analysis performed demonstrated that the displacement of metal from the tube is accompanied by the formation of an annular eddy in the metal. This eddy entrains the lump material and gas that is concentrated in the eddy in the form of a torus reaching the bottom of the ladle and subsequently breaks it into bubbles. The conditions of the formation of a gas-containing eddy and the passage of lump materials through the short tube and into the ladle are studied. An equation is derived to quantitatively estimate these processes. In accordance with the said equation, if bubbling gas (e.g., argon) is used at a flow rate of 50 m^3 , displacing pieces of ferrosilicon 0.02 m in size through a ladle with a tube 0.6 m in diameter requires that the metal be passed into the tube at a rate of at least 0.86 m/s . If no bubbling gas is used, the rate at which the metal is passed into the tube must be increased to 1.34 m/s . Displacing pieces of ferrosilicon 0.05 m in size requires that the metal be added at rates of

1.75 and 2.74 m/s with and without bubbling gas respectively. Figures 3; references 9: 8 Russian, 1 Western.

Increasing the Structural Strength of 20K Boiler Steel by Microalloying and Controlled Rolling

927D0158H Moscow ROSSIYSKAYA AKADEMIYA NAUK: SERIYA METALLY in Russian No 1, Jan-Feb 92 (manuscript received 22 Oct 90) pp 159-164

[Article by M.V. Bobylev, V.B. Kireyev, and A.M. Koresheva, Moscow; UDC 669.14.018.853]

[Abstract] The authors of the study reported herein examined the effect that microalloying 20K steel with up to 0.1 percent vanadium and up to 0.04 percent niobium and using a controlled rolling regimen (i.e., varying the temperature at the end of the rolling process within the range from 750 to 850°C) have on the formation of the structure and properties of the said steel. The steel for the study was melted in a 60-kg induction furnace and cast into three 17-kg ingots. Type 03ZhR burden, ferrovanadium, and metallic niobium in amounts and purities conforming to the specifications established for 20K boiler steel were used as starting materials. The ingots were forged into sheet billets measuring $70 \times 70 \text{ mm}$ and rolled to a thickness of 14 mm in different controlled regimens. The following rolling regimens were used: 1) heating the metal to a temperature of $1,200^\circ\text{C}$, interim cooling to 900°C , rolling in two passes from 70 to 50 mm (with a 15 to 17 percent deformation rate per pass), followed by interim cooling to temperatures of 750 , 800 , and 850°C and 2) rolling sheets to a thickness of 14 mm in five passes (with intervals of 10 to 12 seconds between passes). During the rolling process the rolling temperature was monitored by an FEP-4 photoelectric pyrometer with a precision of $\pm 10^\circ\text{C}$. Analysis of the study specimens revealed that microalloying with vanadium and/or niobium sharply reduces the steel's tendency toward austenite grain growth: The microalloyed steels maintained a grain size of 10 to $20 \mu\text{m}$ and a uniform structure all the way to temperatures of 950 to $1,000^\circ\text{C}$. Reducing the temperature at the end of the rolling process from 850 to 170°C was found to result in a 5 to 10 percent increase in the yield strength of the study 20K boiler steel without significantly affecting its ultimate strength or plasticity. Analysis of the structural strength of the study steel at room temperature revealed that the best combination of short-term strength and plasticity is achieved by controlled rolling with a temperature of 800°C at the end of the rolling process. By controlling the regimen under which type 20K boiler steel is rolled, the researchers were able to increase both its short-term and long-term strength by 10 to 40 percent while maintaining a satisfactory plasticity and resilience. Figures 2; tables 2; references 10: 9 Russian, 1 Western.

The Effect of Alloying on the Kinetics of Carbide Particle Dissolution During the Laser Treatment of Steel

927D0158I Moscow ROSSIYSKAYA AKADEMIYA NAUK: SERIYA METALLY in Russian No 1, Jan-Feb 92 (manuscript received 24 Oct 90) pp 176-180

[Article by D.V. Shtanskiy, I.V. Lyasotskiy, and B.Ya. Lyubov, Moscow; UDC 539.27:548.526:621.9.048.7]

[Abstract] The authors of the study reported herein conducted a theoretical analysis of the effect of alloying on the kinetics of carbide particle dissolution when steel is subjected to laser treatment. Specifically, by using the three-component system Fe-Cr-C as an example, they calculate the changes over time that occur in the carbon and dopant concentration fields of dissolved spherical carbide ($\text{Fe, Cr}_7\text{C}_3$) formations. The changes in the formations' radii while the radiation is falling onto the surface of the metal mass are also calculated. An expression describing the said process is derived. On the basis of their calculations, the authors conclude that the dissolution resistance of the carbide phase in chromium-doped steels is much higher than that of nondoped steels. To confirm the validity of their calculations, the researchers performed a series of experiments in which specimens of ShKh-15 and Kh12M steel were irradiated by 1) a CO_2 laser with a power flux density of 4×10^3 to $4 \times 10^4 \text{ W/cm}^2$ for periods of 0.3 to 1 second and 2) a Kvant pulsed laser with a power flux density of $2 \times 10^4 \text{ W/cm}^2$ for a period of 4×10^{-3} seconds. The rate of heating ranged from 3×10^2 to $3 \times 10^3 \text{ }^\circ\text{C/s}$ in the first and amounted to 2×10^5 in the second case. Layer-by-layer electron microscope analysis of the laser radiation-affected zones of the study specimens were performed with a JEM-200CX scanning electron microscope. A structure with preservation of incompletely dissolved carbide particles was determined to be optimal from the standpoint of the best overall set of mechanical properties. Figures 2; references 13: 9 Russian, 4 Western.

Peculiarities of Structural and Phase Transformations in Ion-Bombarded Inert Steels

927D0159B Moscow FIZIKA I KHIMIYA
OBRABOTKI MATERIALOV in Russian No 1,
Jan-Feb 92 (manuscript received 11 Feb 91) pp 11-15

[Article by O.V. Borodin, V.N. Voevodin, V.I. Krivoshey, I.M. Neklyudov, and P.V. Platonov, Kharkov; UDC 539.16]

[Abstract] An experimental study of EP-838 modified Mn-Cr steel was made concerning dilation, microstructural changes, and phase stability under bombardment by heavy ions, this study having been included in an extensive program to develop new materials featuring low activation by long-life radionuclides for use in thermonuclear reactors. Specimens of this austenitic stainless steel (0.058 percent C, 13.1 percent Mn, 12.4 percent Cr, 4.1 percent Ni, 0.83 percent Al, 0.54 percent Mo, 0.28 percent Si, 0.02 percent N, 0.017 percent P, 0.014 percent S), some having been only cold worked to 30 percent deformation and some having been subsequently austenitized at 1050°C for 30 min, were bombarded with 3 MeV Cr^{2+} ions at temperatures covering the $300\text{--}700^\circ\text{C}$ range. This initially straight

austenitic steel with grains in the $15\text{--}20 \mu\text{m}$ size fraction became defective at rates of $(0.5\text{--}1) \times 10^{-2}$ discompositions/(atom.s) with the percentage dilation peaking to a maximum at temperatures within $600\text{--}635^\circ\text{C}$, at 600°C porosity due to vacancies beginning to develop at doses of 40-50 discompositions per atom in cold-worked specimens and at doses of 50-60 discompositions per atom in austenitized specimens. The dose dependence of dilation indicates a longer incubation period after cold working than after subsequent austenitizing and almost the same steady-state dilation rate after both treatments. Examination in an electron diffractometer has revealed a $\gamma \rightarrow \alpha$ phase transformation with attendant precipitation of Mn_4N and M_{23}X_6 phases with an f.c.c. crystal lattice each at the austenite grain boundaries. Figures 5; tables 2; references 7.

Controlling Steel and Alloy Structure During Suspension Inoculation by Ultradisperse High-Melting Compound Powders

927D0163D Moscow ROSSIYSKAYA AKADEMIYA
NAUK: SERIYA METALLY in Russian No 2,
Mar-Apr 92 pp 168-171

[Article by V.P. Saburov, Ye.N. Khlystov, G.N. Minnekh-anov, Omsk; UDC 669.14.018.28:669.893]

[Abstract] An analysis of the strength theory of crystalline materials shows that in order to harden the metal with extraneous disperse particles, which increase the yield strength without the danger of producing stress concentrators, ultradisperse particles whose shear modulus exceeds that of the alloy matrix are necessary. The process of steel and alloy inoculation with the help of ultradisperse particles (UDP) with a $0.01\text{--}0.5 \mu\text{m}$ degree of dispersion is treated as artificial heterogenation of liquid metal prior to solidification due to the development of concentration inhomogeneities which form a local concentrational supercooling; the latter lowers the energy barrier during the solidification center nucleation. Such oriented melt heterogenation with the formation of a disperse system increases the liquid metal density and viscosity and, likewise, alters its fundamental characteristics. It prevents the growth of columnar crystals, refines the dendritic structure of equiaxial crystals, changes the composition of excess phases and their morphology and topography, and increases the strength and ductility of the casting metal. The nonequilibrium state of the melt system may persist in the solid state. The technical and economic impact from the use of suspension inoculation with ultradisperse powders at the Saturn Scientific Production Association for castings from the VKhChL and ZhS-3DK alloys is a 10 to 15 percent increase in strength and 20 to 100 percent in ductility and a 15 to 20 percent increase in the long-term strength at operating temperatures. Tables 1; references 9.

Mechanism of Electron Excitation in Germanium by Atomic Hydrogen

927D0157B Moscow *POVERKHNOST: FIZIKA, KHIMIYA, MEKHANIKA* in Russian No 1, Jan 92 (manuscript received 7 Feb 89, signed to press 5 Feb 91) pp 28-34

[Article by V.F. Kharlamov, Tomsk Institute of Automatic Control Systems and Radio Electronics; UDC 621.315.529]

[Abstract] Electron excitation in Ge(111) crystals upon adsorption of hydrogen atoms is analyzed on the basis of a phenomenological model which accounts for six processes involving a hydrogen atom (H) and an adsorption center (Z). Four of them are reversible: 1) adsorption of atoms $H + Z \rightarrow HZ$, 2) strengthening of bond $HZ \rightarrow (HZ)$, 5) adsorption of atoms $H + Z \rightarrow (HZ)$, 6) recombination of adsorbed atoms $(HZ) + (HZ) \rightarrow H_2 + 2Z$. Two of them are irreversible: 3) recombination of adsorbed atoms $HZ + HZ \rightarrow H_2 + 2Z$, 4) recombination of adsorbed atoms $HZ + (HZ) \rightarrow H_2 + 2Z$. The two reversible transitions in the reversible $HZ \rightarrow (HZ)$ process are $HZ \rightarrow (HZ)$ and $HZ \rightarrow (HZ) + e + p$ (e- electron in conduction band, p- hole in valence band). The system of equations describing all six process is solved analytically for the rate $J(t)$ of atom to atom recombination and the intensity $I(t)$ of electron-hole states excitation, both as functions of time. Subsequent numerical estimates indicate that this model fits known experimental data. Absence of surface blocking hydrogen molecules owing to their volatility along with saturation of $J(n)$, $I(n)$, and I_L (I_L - intensity of radical- radical recombinational luminescence, n- concentration of atoms in the gaseous phase) indicate that recombination of hydrogen atoms on the crystal surface proceeds according to the Langmuir-Hinshelwood mechanism. Participation of two kinds of adsorbed atoms in the process, some in a short-life state and some in a long-life state, explains not only the step change of J , I , I_L , and I (I- chemical electron emission current) upon removal of the atom source but also the "shears" between $I_L(t)$ and $N(t)$ (N- concentration of adsorbed atoms in the gaseous phase) curves, the initial spikes on all three $I(t)$, $I_L(t)$, I curves when the H-atom flux is large, and the prolonged initial rise of I_L when the H-atom flux is small. The author thanks Yu.N. Rufov, V.V. Styrov, and Yu.I. Tyurin for helpful discussions. References 30.

Effect of Electron Bombardment on Surface Charge of Alkali-Halogenide Crystals

927D0157F Moscow *POVERKHNOST: FIZIKA, KHIMIYA, MEKHANIKA* in Russian No 1, Jan 92 (manuscript received 10 Jul 90, signed to press 18 Oct 90) pp 88-91 [Article by B.G. Atabayev, N.N. Boltayev, and S. Gaipov, Institute of Electronics, UzSSR Academy of Sciences, Tashkent; UDC 537.533+537.534]

[Abstract] An experimental study of NaCl and KCl crystals with color centers was made concerning the effect of electron bombardment on their surface charge. The (100) facets of NaCl and KCl single crystals were first bombarded at room temperature with a 3 keV electron beam

having a current density of the order of $1 \mu A/cm^2$. This bombardment produced F-centers and M-centers in the surface layer, their concentration being varied by varying the bombardment dose (time) and the accumulated surface charge then being removed by heating. The crystals, with some defects removed and their surface cleaned by soaking at about $350^\circ C$ for two to three hours, were then bombarded with various electron beams covering the 60 to 1000 keV energy range and thus electron doses up to about $10^{19}/cm^2$. Crystals with color centers and, for reference, also "pure" crystals were treated in this way. The stationary potential of their thus charged surface was determined from the shift of the energy spectrum of secondary electrons, this shift being measured with a 127° Hughes-Rozhanskiy cylindrical capacitor-analyzer and depending on the bombardment dose. Also the secondary electron emission was measured at the same time, for an evaluation of its dependence on the bombardment dose. The results indicate that buildup of positive surface charge on all these crystal during electron bombardment is due to secondary electron emission by them. The potential of a surface thus charged by electrons of a certain energy level decreased as the bombardment dose was increased and with it the concentration of color centers, evidently owing to a decreasing yield of secondary electrons and to capture of extra electrons by color centers. Thermoluminescence analysis of color centers revealed that electron bombardment had produced F-centers in NaCl crystals and M-centers as well as F-centers in KCl crystals. This agreed with the results of measurements, a larger net negative surface charge and a lower resultant positive surface potential having been read on KCl crystals. Figures 3; references 7.

Temperature-Dependent Concentration Profiles of Nitrogen Implanted in Be, Si, Fe, Nb

927D0157FG Moscow *POVERKHNOST: FIZIKA, KHIMIYA, MEKHANIKA* in Russian No 1, Jan 92 (manuscript received 29 Jan 90, signed to press 25 Feb 91) pp 115-121 [Article by K.Sh. Chokin and Ye.Yu. Pereverzev, Institute of Nuclear Physics, KaSSR Academy of Sciences, Alma-Ata; UDC 539.219.3:621.315.592]

[Abstract] An experimental study of nitrogen ion implantation into thin surface layers of Be, Si, Fe, and Nb targets was made, concerning the behavior of the nitrogen impurity atoms and the dependence of their concentration profiles on the temperature of subsequent isothermal annealing of those layers. Preparation of the targets consisted of sputtering them with one keV Xe^+ -ions, cleaning their surface, and a reducing heat treatment at 900° for one hour. Nitrogen implantation was then done with a normally incident beam of 1.5 keV N-ions at a $20^\circ C$ temperature, till the nitrogen content on the surface of the target had reached 5 to 8 atom. percent. The targets were then isothermally annealed at successively higher temperatures from $100^\circ C$ to 800° for 30 minutes at each, with the nitrogen content as well as the Be, Si, Fe, and Nb content in the respective targets being continuously monitored throughout each annealing, which was followed by cooling

and holding at room temperature for measurement of the depthwise N-concentration profile by the layerwise etching method in an LAS-2000 Auger spectrometer. The results indicate a unidirectional migration of implanted N-atoms toward the target surface, this migration intensifying as the temperature is raised. Selection of an adequate simple model for description and theoretical analysis of the intricate migration processes involved in nitrogen implantation layers is very difficult, although various diffusion mechanisms have been proposed, so that the search of such a model is waived. The mean local impurity velocity $V(x)$ and the rate of change of impurity concentration $\delta C(x,t)$ during annealing at some constant temperature are, instead, calculated on the basis of the ample experimental data and in the one-dimensional approximation in accordance with Fick's first law $V(x) = I(x,t)/C(x,t)$ and Fick's second law $\delta C(x,t)/\delta t = \delta[V(x)C(x,t)]/\delta x$ respectively (I -impurity flux intensity, t -time). The results indicate that ion implantation into such targets is accompanied by strong perturbation of target atoms. Nitrogen atoms evidently migrate faster in Fe and Be targets than in Si and Nb targets so that relaxation processes in Fe and Be targets influence the final N-concentration profile in these targets much more strongly, causing it to peak near the surface, than these processes do in Si and Nb targets. Figures 4; references 15.

Unevenness of the Distribution of the Components of AKS Additive in Tungsten Wire

927D0158J Moscow ROSSIYSKAYA AKADEMIYA
NAUK: SERIYA METALLY in Russian No 1,
Jan-Feb 92 (manuscript received 3 May 90) pp 186-188

[Article by A.M. Bogomolov, A.A. Kalkov, I.I. Litvinova, and L.G. Kabakova, Chirchik; UDC 669.27-426:539.56]

[Abstract] The authors of this concise report used the method of neutron activation analysis to determine the content of the elements of standard AKS additive in tungsten tri- and dioxide powders, in metallic tungsten powder, and in compact tungsten (small bars of tungsten). The content of Al, Si, and K (i.e., the components of standard ASK additive) in the study specimens was determined by using an NG-200 neutron generator and the VVR-SM nuclear reactor of the Nuclear Physics Institute of the UzSSR Academy of Sciences. The degree of unevenness of the elements' distribution was estimated on the basis of the coefficient of variation. A degree of unevenness in the distribution of the aluminum, silicon, and potassium contained in all phase components of the reduction chain (i.e., $WO_3 \rightarrow WO_2 \rightarrow \alpha-W$) as well as in compact tungsten was discovered. The coefficient of variation for aluminum and silicon ranged from 30 to 50 percent and reached 70 percent for potassium in compact tungsten. Pyrophyllite, sillimanite, and corundum were discovered to be the predominant phases of AKS additive in compact tungsten. On the basis of their studies, the researchers concluded that the formation of micropores in tungsten filaments is evidently related to the high degree of unevenness of the distribution of Al, Si, and K that occurs when the said elements are added to tungsten trioxide in the form of AKS additive. References 7: 6 Russian, 1 Western.

New Compounds With $PuNi_3$ Structure in Rare Earth Metal-Cu-Al Systems

927D0163H Moscow ROSSIYSKAYA AKADEMIYA
NAUK: SERIYA METALLY in Russian No 2,
Mar-Apr 92 pp 227-230

[Article by Yu.B. Kuzma, B.M. Stelmakhovich, V.S. Babi-zhetskii, Lvov; UDC 669.3.71.851+548.736]

[Abstract] New compounds are discovered in studies of (Ho, Yb, Lu)-Cu-Al systems near the $MeCuAl_2$ composition (Me is the rare earth metal (RZM)); consequently, an attempt is made to investigate the crystal structure of $MeCuAl_2$ intermetallic compounds and to search for isostructural compounds in $MeCu$ -Al systems with other rare earth metals. Samples for the study are fused from at least 0.995 pure rare earth metal, 0.9999 pure electrolytic Cu, and 0.9999 pure Al in an electric arc furnace in an atmosphere of purified Ar on a copper water-cooled bottom. The crystal structure of the $HoCu_{0.9}Al_{2.1}$ compound is examined by X-ray phase, X-ray structural, and microstructural analyses and the coordination numbers and coordination polyhedrons of atoms in the compound structure are analyzed. The diffraction patterns, atomic spacing δ , and lattice constants are calculated and the behavior of the lattice constants as a function of the REM ordinal number is plotted. Isostructural compounds with an yttrium group REM are produced and the valence state of Me atoms in the compound is determined. The phase equilibria diagram of the Y-Cu-Al system is examined partially to a 0.20 molar Y fraction. Figures 1; tables 3; references 7.

Vacuum Refining as Method of Producing High-Purity Aluminum

927D0165E Moscow VYSOKOCHISTYYE
VESHCHESTVA in Russian No 2, Mar-Apr 92
pp 84-90

[Article by A.V. Vakhobov, F.U. Obidov, M.K. Bik-timirova, Chemistry Institute, Dushanbe; UDC 669.071.543]

[Abstract] The need to remove various nonmetallic impurities, primarily hydrogen, from electrolytically refined aluminum and the scarcity of published data on this problem prompted an investigation of the process of vacuum liquid aluminum exposure with subsequent oriented crystallization for the purpose of refining. The study is carried out under lab and commercial conditions at the Tadzhik Chemistry Institute and at a pilot production enterprise of especially pure substances. To this end, 1,000 mm long ingots with a 70 mm diameter are machined, then degreased, surface-pickled in aqua regia, washed in distilled water, dried, placed into graphite analysis boats, and loaded into stainless steel tubes with a $1 \cdot 10^{-5}$ mm Hg vacuum. Liquid Al is exposed to 850°C for 25 to 30 hours, then to 750-780°C for 10 hours. Then the oriented crystallization process is conducted, and the temperature is gradually decreased at various rates. The behavior of the temperature and cooling rate during the vacuum refining and highly volatile impurity distribution during the vacuum exposure of liquid aluminum are plotted. The

easily volatile component concentration in aluminum after the vacuum exposure, the impurity concentration in the original A995 Al and in the graphite container before and after the vacuum degassing, and the poorly volatile impurity distribution in the ingot after oriented crystallization are summarized. It is shown that the oriented crystallization process is necessary not only for removing impurities, but also for equalizing the ingot cross section. After both process stages, the final Al purity reaches 99.999 percent by mass, confirming the efficacy of the vacuum refining method. Figures 2; tables 3; references 12: 10 Russian, 2 Western.

High-Purity Silicon for Ionizing Radiation Detectors

927D0165F Moscow VYSOKOCHISTYYE
VESHCHISTVA in Russian No 2, Mar-Apr 92
pp 134-140

[Article by K.N. Neymark, Yu.V. Trubitsyn, I.F. Chervonyy, Zaporozhye Integrated Titanium Magnesium Works; UDC 621.315.592]

[Abstract] The need for high-purity detector-grade silicon for use in experimental physics, process monitoring systems, and radiation counters, and especially for silicon with high resistivity (UES) uniformly distributed in the transverse single crystal cross section, with a long minority charge carrier (NNZ) life, and an absence of dislocations and swirl defects is noted, and the shortcomings of existing methods, e.g., floating zone melting (BZP) are stressed. The need to ensure a high purity level at all process stages is identified, and the principal features of the high-purity silicon production methods are outlined. The characteristics of the principal impurities in Si and the impurity concentration in argon—the medium in which silicon single crystals are grown—are summarized, and the parameters of the floating zone melting process used for producing single crystals with various types of microdefects are examined. The characteristics of high-purity single crystals produced at the Zaporozhye Integrated Titanium Magnesium Works (ZTMK) are cited. The radiation resistance of single crystals of silicon after neutron transmutation alloying (NTL) is examined at the Kiev Nuclear Research Institute (KIYaI). The production equipment characteristics and testing methods are described. D-type microdefects are found to be the most stable to thermal exposure up to 1,300°C. The results demonstrate that Si single crystals produced at the ZTMK have high electrophysical properties. Tables 4; references 18: 13 Russian, 5 Western.

Today's State of High-Purity Metal Fluoride Production for Fiber Optics

927D0165G Moscow VYSOKOCHISTYYE
VESHCHISTVA in Russian No 2, Mar-Apr 92
pp 105-114

[Article by V.I. Zvereva, Chemistry Scientific Research Institute at the Nizhny Novgorod State University; UDC 661.482:667.529]

[Abstract] The rising demand for high-purity fluorides of metals for making optical materials for fiber optics, laser materials, and other optical media used in the fields of communications and scientific instruments, and particularly for fluorozirconate glass—one of the most promising materials for fiber optics—is discussed. The leading companies producing fluoride of metals, primarily rare earth metals and zirconium, hafnium, barium, aluminum, sodium, lithium, and beryllium in the United States, Great Britain, France, Germany, and Japan and their particular emphases are listed, and the purity of metal fluorides produced by various companies is summarized. The purity and production cost of metal fluorides produced by various companies are compared, and metal fluoride export and import dynamics in 1989-1990 are examined. It is shown that the volume of metal fluoride trade on the world market is on the rise; Japan and Germany are now producing highly competitive metal fluorides. The rising cost of metal fluorides is noted. The author is grateful to the staff of the Nizhny Novgorod Scientific Production Information Implementation center "Patenservis", particularly L.S. Pozin, N.T. Bishletov, and T.P. Zubkov for patent and opportunity research. Tables 8; references 62: 19 Russian, 43 Western.

High-Purity Silane Silicon-Based Ionizing Radiation Detectors

927D0165H Moscow VYSOKOCHISTYYE
VESHCHISTVA in Russian No 2, Mar-Apr 92
pp 141-143

[Article by Yu.A. Nechuneyev, G.V. Ladonychev, A.G. Petrik, E.S. Falkevich, A.V. Mokrushin, High-Purity Substance Chemistry Institute at Russia's Academy of Sciences, Nizhny Novgorod and Zaporozhye Integrated Titanium Magnesium Works; UDC 621.376.234]

[Abstract] The effect of various silicon characteristics on the quality of ionizing radiation detectors with a high energy resolution is discussed, and a new method of producing high-purity silicon using the silane technology developed at the Zaporozhye Integrated Titanium Magnesium Works is outlined. A series of high-purity silicon specimens produced by such a technology is investigated; to this end, the electric resistivity, charge carrier mobility, noncompensated charge carrier concentration, conduction type, deep center density, and dislocation density are measured, and the most representative values of these quantities are summarized. The dependence of the reverse current on the applied voltage and the ^{238}Pu α -source spectra recorded by two types of detectors are plotted. It is noted that a small increase in the deep center concentration leads to a noticeable deterioration of the detector characteristics. The study demonstrates that silicon produced by the silane technology with a $10\text{ k}\Omega\text{cm}$ resistivity and an $n \cdot 10^{12}\text{ cm}^{-3}$ noncompensated charge carrier mobility is suitable for making ionizing radiation detectors with a high energy resolution. Figures 3; tables 1; references 2.

Effect of Pulsed Heat Treatment on Electrophysical Properties of Zr-Si Interface

927D0157C Moscow *POVERKHNOST: FIZIKA, KHIMIYA, MEKHANIKA* in Russian No 1, Jan 92 (manuscript received 14 Dec 90, signed to press 19 Dec 90) pp 56-60

[Article by A.M. Chaplanov, A.N. Shibko, T. Dyakov, and G. Mladenov, Institute of Electronics, BSSR Academy of Sciences, Minsk; UDC 621.373.826. 038.825]

[Abstract] An experimental study of the Zr-Si composite was made concerning the effect of pulsed heat treatment on the metal-semiconductor interface and its electrophysical properties. About 100 nm thick films of fine-disperse polycrystalline Zr with grains in the 20-30 nm size fraction were deposited by vacuum evaporation on n-Si(100) substrates at an about 373 K temperature, covering a surface area of $5 \times 5 \text{ mm}^2$. Some specimens were treated with a $1.06 \text{ }\mu\text{m}$ laser beam scanning them under a vacuum of 0.3 mPa for a period of three seconds, the energy density being varied over the 1.7-2.2 J/cm² range. Some specimens were treated with an electron beam under an accelerating voltage of 30 kV, the energy density being varied over the 5-40 J/cm² range. Structural and phase transformations occurring as a result of each treatment were examined by the method of Rutherford backscattering spectrometry as well as under an electron microscope and in an electron diffractometer. Pulsed heat treatment of the composite material with either a laser beam or an electron beam was found to move the film closer to a state of equilibrium, upon migration of intergranular boundaries and attendant growth of grains. As the energy density of laser-beam treatment was raised above 1.7 J/cm², a ZrSi phase and then also a ZrSi₂ phase appeared with eventually no metallic Zr remaining in the interface after treatment with an energy density of 2.2 J/cm². Treatment with an electron beam caused formation of a Zr₂Si phase, a Zr₃Si₂ phase, and a Zr₅Si phase in the interface when the energy density was 5 J/cm², also formation of a ZrSi phase with no metallic Zr remaining in the interface when the energy density was 10 J/cm², formation of only a ZrSi phase and a ZrSi₂ phase with no metallic Zr remaining in the interface when the energy density was 20 J/cm², and only a ZrSi₂ phase with no metallic Zr remaining in the interface when the energy density was 40 J/cm². Backscattering measurements revealed a distinct metal-Si separation by a SiO₂ interlayer, indicating a maximum oxygen content at a depth of about 100 nm under the film surface. Increasing the energy density of pulsed heat treatment had evidently caused silicon to diffuse through that growing interlayer into the metal film so that ZrSi₂ was eventually formed. The current-voltage characteristics of the initial Zr-Si junction and of the ZrSi₂/SiO₂/Si junction were measured so that the magnitude of the Schottky barrier could also be determined. Figures 2; tables 4; references 6.

Photochemical Etching of Silicon With Continuous-Wave Laser Radiation

927D0157D Moscow *POVERKHNOST: FIZIKA, KHIMIYA, MEKHANIKA* in Russian No 1, Jan 92 (manuscript received 28 Sep 90, signed to press 4 Jan 91) pp 70-76

[Article by Ye.A. Volkova, A.M. Popos, O.B. Popovicheva, and T.V. Rakhmilov, Scientific Research Institute of

Nuclear Physics at Moscow State University imeni M.V. Lomonosov, Moscow; UDC 661.185:621.794]

[Abstract] An analysis of laser-induced etching of silicon in a gaseous atmosphere of Cl₂ molecules is performed on the basis of a mathematical model describing the concentration distributions of chlorine radicals N_{Cl}•, of chlorine molecules N(Cl₂), and of photoelectrons n_e in solid Si under its surface. The model simulates the conditions of an experiment (P. Mogyurosi, K. Piglmayer, K. Kullmer, and D. Bauerle; *APPLIED PHYSICS A* Vol 45, 1988) involving treatment of Si(100) with a Kr⁺-laser ($\lambda = 351 \text{ }\mu\text{m}$) and with an Ar⁺-laser ($\lambda = 457.9 \text{ }\mu\text{m}$, $488 \text{ }\mu\text{m}$, $514.5 \text{ }\mu\text{m}$) in such an atmosphere. The two competing processes, namely generation of Cl radicals by photodissociation of Cl₂ molecules and annihilation of Cl radicals as a results of their recombination, are described by a two-dimensional equation of diffusion kinetics (in cylindrical coordinates r, z and time t) for the rate of change of radical concentration distribution $\delta N(\text{Cl})(r, z)/\delta t$, with a third term on the right-hand side implicating both intensity and wavelength of the incident laser radiation as well as its reflection by the Si surface. This equation is solved for boundary conditions of zero Cl flux at the Si surface and at a far distance from it. The evolution of the photoelectron concentration distribution n_e(r, z) is described by an analogous two-dimensional equation of diffusion kinetics for the rate of change of photoelectron concentration $\delta n_e(r, z)/\delta t$, a second term on the right-hand side implicating Auger recombination of electrons in solid Si and a third term on the right-hand side implicating absorption of laser radiation by solid Si and its reflection by the Si surface. This equation is solved on the assumption of a zero electron flux at the Si surface, insofar as $(n_e \gg N(\text{Cl}_2))$. The two equations have been solved numerically with the aid of known experimental data, as a basis for estimating the much lower than unity probability of Cl-Si interaction which results in photochemical etching and thus depends on the intensity of incident laser radiation, also for a determination of the etching rate proportional to the number of Si atoms knocked off the surface by one Cl atom. Addition of a small amount of a gas such as HBr readily reacting with Cl radicals ($\text{Cl} + \text{HBr} \rightarrow \text{HCl} + \text{Br}$) under normally incident laser radiation was found to result in a much more uniform distribution of those radicals and to thus enhance the etched surface profile for formation of structural patterns with a micrometric spatial resolution. Figures 5; references 11.

Dependence of Nonhomogeneity of Thin Glass Films Produced by High-Frequency Sputtering on Chemical Composition of Substrate Glass

927D0157E Moscow *POVERKHNOST: FIZIKA, KHIMIYA, MEKHANIKA* in Russian No 1, Jan 92 (manuscript received 31 Jul 90, signed to press 24 Jan 91) pp 78-82

[Article by .S. Malashchenko, V.P. Redko, L.Ye. Starovoytov, and A.V. Khomchenko, Mogilev Department, Institute of Physics, BSSR Academy of Sciences; UDC 539.23+666.1.053.65]

[Abstract] An experimental study of thin films of optical glass deposited by high-frequency sputtering on glass substrates to form dielectric waveguides or interference coatings was made, concerning the dependence of their optical nonhomogeneity on the chemical composition of the substrate. For this purpose 0.54-0.59 μm thick films of BK10 borosilicate glass were deposited on LK6, LK7, K2, and quartz glass substrates and 1.11-1.20 μm thick films of TK20 thalliosilicate glass were deposited on TK9, TK14, TK20, LK7, and K8 substrates by h-f sputtering in an Ar + O₂ atmosphere under a total pressure of 0.1 Pa (P O₂ = 0.02 Pa), all films from both BK10 and TK20 target being deposited on all substrates simultaneously so as to ensure identical process conditions. The targets were under a constant 250 V self-bias voltage in a triode configuration, the plasma current was maintained at 2.6 A, and the temperature of the substrates did not exceed 200°C. The refractive index and its dispersion were measured by the waveguide method with a prismatic coupling element and with resonance excitation using light of 450-650 nm wavelengths, the measurement error not exceeding 10^{-4} . The thickness of films was measured with a relative error not larger than 2 percent. The index profile across the film thickness was then evaluated in two ways: 1) by the Wentzel-Kramers-Brillouin waveguide method with a polystyrene film (refractive index $n = 1.58$) deposited as reference on the original thin-film structure, 2) by ellipsometry with a compensator-ellipsometer and 0.63 μm light incident at five different angles covering the 45-57° range. Calculations based on a triple-layer "transition layer - glass film - affected surface layer" structure on a substrate yield a fairly close agreement with the experimental data. The different index distributions over the film thickness on different substrates are convincing evidence that the degree of optical nonhomogeneity of a thus deposited glass film depends on the chemical composition of the substrate glass, the thickness of the nonhomogeneous film layer and the variation of the refractive index within that layer being evidently minimizable by matching the film glass and substrate glass compositions. Figures 2; tables 2; references 7.

Change in Properties of Carbon Materials Under Neutron Bombardment

927D0159A Moscow FIZIKA I KHIMIYA
OBRABOTKI MATERIALOV in Russian No 1,
Jan-Feb 92 (manuscript received 31 May 91) pp 5-10

[Article by Yu.S. Virgilyev, Moscow; UDC 621.039.532.21]

[Abstract] Experimental data on neutron bombardment of completely nongraphitized reactor carbon and attendant changes in its properties are reviewed and analyzed, this material being remarkable on account of the very low level of neutron bombardment at which its secondary dilation begins. Billets of this intermediate product (density 1.55 g/cm³, dynamic modulus of elasticity 11.5 +/- 1.1 GPa longitudinally and 7.8 +/- 1.0 GPa transversely, electrical resistivity 43.1 +/- 1.5 $\mu\text{ohm.m}$ longitudinally and 58.6 +/- 4.0 $\mu\text{ohm.m}$ transversely, graphitization level 0) were bombarded by neutrons with an up to $6 \times 10^{21} \text{ cm}^{-2}$ fluence

of neutrons with energy higher than 0.18 MeV, at temperatures ranging from 340 K to 1200 K. After each bombardment the density and the electrical resistivity of the material were measured, also the relative change in billet height; whereupon the billets were tested for compressive strength and dynamic modulus of elasticity for an evaluation of the dependence of all these properties on both the temperature and the fluence of bombarding neutrons. The results of this evaluation indicate a much larger initial shrinkage owing to aggregation of spheroidal microparticles and a much larger subsequent secondary dilation of nongraphitized material than of graphitized one, secondary dilation also beginning at a much lower threshold level of neutron fluence. As secondary dilation of nongraphitized reactor carbon continues, both its dynamic modulus of elasticity and compressive strength decrease and its electrical resistivity increases. Figures 2; tables 1; references 14.

Structural Changes on Silicon Surface Under Laser Radiation

927D0159D Moscow FIZIKA I KHIMIYA
OBRABOTKI MATERIALOV in Russian No 1,
Jan-Feb 92 (manuscript received 28 Mar 91) pp 50-55

[Article by A.F. Banishev and M.M. Novikov, Moscow Oblast; UDC 537.311.322]

[Abstract] An experiment with silicon single crystals was performed involving their treatment with 1.06 μm radiation of a YAG:Nd³⁺ solid-state laser in pulses of 1.6 ms duration and up to 3 J energy. Structures forming in the solid phase and in the melt were tracked and examined simultaneously by two independent methods: one based on infrared radiation emission from the laser-affected zone, one based on specular reflection and reflection diffraction of a probing He-Ne laser beam by the treated silicon surface. The apparatus for examination by the first method included a Ge:(Au) infrared radiation detector, a monochromator, and an S9-8 high-speed oscilloscope. The apparatus for examination by the second method included two waveguides, for specularly reflected radiation and for diffracted radiation respectively, also a photomultiplier, which recorded specular reflection as a function of time for an indication of the onset of fusion. The silicon surface after laser treatment was also examined under a microscope and in a polarimeter. The results of these examinations indicate that: 1) laser pulses with energy up to 8.5 J/cm² have not caused any structural changes on the silicon surface; 2) laser pulses with energy of 8.5-25.5 J/cm² have produced a two-dimensional periodic cellular surface structure, as a result of periodic local fusion according to dislocation theory; 3) laser pulses with energy of 25.5-34.5 J/cm² have fused the silicon surface; 4) laser pulses with energy of 34.5-50 J/cm² have induced formation and development of two kinds of periodic lattices, one whose period and orientation are determined by the configuration of the crystallographic axes after ordering of lattice cells has occurred in the melt and one of the interference type whose period and orientation are determined by the laser radiation; 5) laser pulses with energy higher than 50 J/cm² have induced a sequence of processes all occurring within the duration of an incident pulse,

namely formation of a periodic cellular structure → fusion of the surface → formation of two periodic lattices → erasure of the periodic pattern. The authors thank V.I. Yemelyanov and A.B. Yevseyev for discussing the results. Figures 3; references 9.

Properties of Molten Slag in Thermal Reprocessing of Radioactive Waste on Base of Shaft Furnace

927D0159F Moscow FIZIKA I KHIMIYA
OBRABOTKI MATERIALOV in Russian No 1,
Jan-Feb 92 (manuscript received 13 Sep 19) pp 68-70

[Article by S.A. Dmitriyev, S.V. Stefanovskiy, F.A. Difanov, and N.A. Knyazev, Moscow; UDC 621.039.73]

[Abstract] Reprocessing solid radioactive waste in shaft furnaces with fuel-plasma heating is considered, the main advantage of this is method being that it yields an inorganic liquid slag which can be poured into containers and buried without prior reprocessing. This eliminates *in situ* casting of residual ash and avoids drift of solid particles into the gas scrubbing system, with only 2 percent or less of radioactive nuclides escaping. In an experimental study various solid radioactive waste items (wood, paper, animal carcasses, contaminated laboratory ware, rubber wear) were put in paper bags and dumped into the shaft of furnace heated by two air-arc plasmatrons operating with 0.3-0.4 excess air. The temperature in the lower part of the furnace was maintained at 1500-1700°C so as to ensure melting of the ash residue and flow of the fluid slag down the inclined hearth into containers. Samples of molten slag were then analyzed by the IAEA method for macrocomponents, radionuclides, and hydrolytic stability. The analysis yielded FeO_x (8.8-43.5 wt. percent), SiO_2 (27.3-35.7 wt. percent), Al_2O_3 (8.3-25.7 wt. percent), CaO (11.5-15.3 wt. percent), P_2O_5 (3.0-10.2 wt. percent), K_2O (2.4-6.2 wt. percent), MgO (2.4-6.0 wt. percent), Cr_2O_3 (0.8-4.3 wt. percent), Na_2O (1.4-3.4 wt. percent), TiO_2 (0.4-1.0 wt. percent), and radionuclides ^{137}Cs , ^{90}Sr , ^{60}Co , ^{59}Fe . Samples were tested for dynamic viscosity at 1400°C (20-60 Pa.s). Solidified slag was black and contained metallic inclusions from the original waste material. Samples were tested for density (1800-5000 kg/m³) and compressive strength (1-2 kN/mm²). The radionuclides were found to have been leached at rates decreasing in the $\text{Cs} > \text{Sr} > \text{Co} > \text{Fe}$ order, none exceeding 10⁻⁵ g/(cm² in 24 hours. According to the results, up to 99 wt. percent of radionuclides in solid waste can be retained in molten slag for immediate burial without prior stabilization. In addition to its other aforementioned advantages, this method is thus also much more efficient than disposal of solid radioactive waste by burning. Tables 2; references 5.

'Dry' Photoanodic Microtreatment of Semiconductors With Laser Beam

927D0159H Moscow FIZIKA I KHIMIYA
OBRABOTKI MATERIALOV in Russian No 1,
Jan-Feb 92 (manuscript received 17 Oct 90) pp 99-102

[Article by D.T. Alimov, V.M. Kosov, and V.V. Yakovina, Tashkent; UDC 621.315.592:546.28]

[Abstract] An experimental study of photoanodic oxidation of semiconductors in a cold plasma by means of a laser beam was made for an evaluation of this "dry" method of their microtreatment versus the "wet" method, considering only formation of nonvolatile transparent oxides of the intrinsic semiconductor material. Specimens of n-GaAs ($n \approx 10^{17} \text{ cm}^{-3}$) and p-GaAs ($p \approx 10^{18} \text{ cm}^{-3}$) substrates were anodized according to the three-electrode scheme, in the galvanostatic mode and in the potentiostatic mode, in an Ar + O₂ gas mixture under pressure of about 0.1 torr during glow discharge with a discharge current within 5-10 mA while also being irradiated by a He-Ne laser with a power density varied up to 1 W/cm² with 1.96 eV photons (absorption band of intrinsic GaAs) or 1.07 eV photons (absorption band of extrinsic GaAs), both levels being within the window in the oxide. The thickness of the oxide layers outside the laser spot (d) and within the laser spot ($d + \Delta d$) was measured with an LEF-3M ellipsometer. Irradiation with 1.96 eV light quanta was found to accelerate oxidation of GaAs in its plasma, the spatial selectivity ($\Delta d + d$)/ d decreasing as the oxide layer was growing on an n-GaAs substrate and only slightly changing as the oxide layer was growing on a p-GaAs substrate, while irradiation with 1.07 eV photons did not influence the kinetics of GaAs oxidation. Decreasing the irradiation power density from 1 W/cm² to 0.1 W/cm² lowered the selectivity on n-GaAs substrates somewhat and on p-GaAs substrates to zero. Switching from galvanostatic to potentiostatic anodization did not appreciably affect the selectivity. Some specimens were oxidized in a standard electrolyte, mixture of ethylene glycol and aqueous 4 percent citric acid in a 3:1 ratio. The selectivity of "wet" microtreatment was found to reach a maximum of 20 on n-GaAs substrates potentiostatically photoanodized while irradiated with 1.96 eV photons and not to be controllable by irradiation on p-GaAs substrates. The photo-e.m.f. on n-GaAs substrates during photoanodization in the electrolyte reached 50 V, a one order of magnitude higher level than during their "dry" photoanodization. The advantage of "dry" photoanodization is its positive effectiveness in microtreatment of p-type semiconductors, the spectral selectivity of such a microtreatment of p-GaAs substrates during their oxidation indicating a direct role of photoholes in "dry" photoanodization. Figures 1; references 11.

Removing Freon-14 Microimpurity From Krypton by Adsorption

927D0165C Moscow VYSOKOCHISTYYE
VESHCHESTVA in Russian No 2, Mar-Apr 92
pp 50-53

[Article by T.A. Kuznetsova, Ye.N. Yegorov, A.M. Tolmachev, Moscow State University imeni M.V. Lomonosov; UDC 541.183]

[Abstract] The dependence of the separation and equilibrium coefficients on the nature of the adsorbent, temperature, and micropore volume space factor of the adsorbent in the krypton-freon-14 system is investigated with respect to the inert gas purification methods. Crystalline NaX zeolite, CaA zeolite with a 20 percent binder composition, and BAU

carbon are used as the adsorbents. The mixture is analyzed in a Tsvet-530 chromatograph column. The values of the separation coefficient and specific purified krypton amount after adsorption of the mixture at a 0.101 MPa pressure using various adsorbents as a function of temperature are summarized; the temperature dependence of the equilibrium coefficient during adsorption by NaX and CaA and the dependence of separation and equilibrium coefficients during adsorption on the volume filling factor of NaX and CaA zeolite micropores are plotted. Zeolites are shown to be the most selective to freon-14; using one kg of commercial NaX zeolite at 120K, one can purify up to 2,000 liters of krypton to a residual freon-14 concentration of $<1 \cdot 10^{-4}$ mol. percent, i.e., the threshold detection limit of the gas chromatograph analyzer. If a desiccated NaX zeolite is used, it is possible to purify up to 3,300 liters of krypton from CF_4 microimpurity. Figures 2; tables 1; references 9: 8 Russian, 1 Western.

Removing Oxygen Impurity From Tellurium Used for Optical Material Synthesis

927D0165D Moscow VYSOKOCHISTYYE
VESHCHESTVA in Russian No 2, Mar-Apr 92
pp 76-79

[Article by A.B. Lobanov, K.A. Pavlova, Ye.A. Kis-litskaya; UDC 666.113.32]

[Abstract] The need to decrease the optical losses of infrared optical materials, including chalcogenide glass, in the 8-14 μm band, particularly on the 10.6 μm wavelength, is identified, and attention is focused on glass with a refractive index on the order of 3.0 containing large amounts of Te and Tl. The issue of improving these types of glass by purifying technical tellurium and removing its oxides in order to decrease absorption losses is considered, and the characteristics of the principal oxygen-containing impurities are examined. The possibility of removing oxides by heat treating the charge is investigated. Transmission spectra of As-Se-Te system glass synthesized from the initial reagents without an additional purification, from reagents distilled beforehand, and from a charge purified by the proposed heat treatment method are plotted and discussed. The conclusion is drawn that by using a variable heating condition, it is possible to reduce tellurium from TeO_2 with the help of other charge constituents which form new, more volatile oxides easily removed by purification. A sample charge is used to produce a glass with a $7 \cdot 10^{-3} \text{ cm}^{-1}$ absorptance. The results demonstrate that tellurium purified by heat treatment can be used for synthesizing chalcogenide glass and for developing other optical materials, e.g., CdTe and ZnTe crystals. Figures 1; references 3.

Chemical Reaction of Copper Sulfate With a Collective Copper-Zinc Concentrate

927D0158C Moscow ROSSIYSKAYA AKADEMIYA
NAUK: SERIYA METALLY in Russian No 1,
Jan-Feb 92 (manuscript received 12 Nov 90) pp 24-28

[Article by N.V. Serova, M.P. Lysykh, T.V. Olyunina, V.I. Goryachkin, A.V. Medvedev, and V.A. Kukoyev, Moscow; UDC 553.43'446:669.2/8.053.4]

[Abstract] The authors of the study reported herein examined the hydrothermal reaction of copper sulfate with a copper-zinc concentrate used to precipitate copper at 190°C from a solution after autoclave leaching. The experiments were conducted in an autoclave in a helium atmosphere with a partial helium pressure of about 0.2 MPa at a temperature of 160 to 190°C for one hour. The open-type turbine mixer used was rotated at a speed of 22.5 s⁻¹. The following were used in the experiments: 1) a collective copper-zinc concentrate (20.3 percent Zn, 8.5 percent Cu, 23.7 percent Fe, 37.1 percent S, and 1.8 percent Pb); 2) a model copper sulfate solution (19.0 g/l copper and 4.5 g/l sulfuric acid); and 3) a leached pulp of the said concentrate containing 88.0 to 92.5 g zinc/l, 2.3 to 1.62 g copper/l, and 16.1-27.5 g iron/l in solution as well as 8.25-0.8 percent zinc, 10.0-15.3 percent copper, 31.0-34.3 percent iron, and 33.7-38.4 percent sulfur in its solid component. Analysis of the chemical reactions of the aforesaid materials revealed that the depth of precipitation of copper from a solution and the extraction of zinc and iron from it increased as the reaction temperature was increased. The cake was found to be enriched in copper and depleted of zinc and iron. A temperature of 190°C was found to be a suitable temperature for precipitating copper. Reducing the ratio of concentrate to solution at the said temperature was found to result in an increase in zinc extraction to the solution and a reduction in the degree of copper precipitation. The results of the experiments reported herein are basically in agreement with data published elsewhere. Petrographic, X-ray phase, chemical phase, and X-ray spectral microanalysis studies all revealed the following to be present in the sediments remaining after the experiments using the concentrate and model solution: pyrite, sphalerite, chalcopryite, covellite, chalcocite, regenerated sulfides, and elementary sulfur. Analysis indicated that as the ratio of the starting sum of copper sulfides and zinc to the dissolved copper decreases, there is a significant increase in the content of chalcocite in the cake and a significant decrease in the content of sphalerite and chalcopryite, with the covellite content remaining essentially unchanged. After discussing their findings in light of other publications on the study reaction, the authors conclude that the mechanism of the reaction of copper sulfate with sulfides under hydrothermal conditions is so complex that it cannot yet be described definitively. Table 1; references 12; Russian.

The Theory and Practice of the Transfer of Ultrasound Vibrations to Molten Metal Through a Waveguide Wire

927D0158F Moscow ROSSIYSKAYA AKADEMIYA
NAUK: SERIYA METALLY in Russian No 1,
Jan-Feb 92 (manuscript received 8 Oct 90) pp 81-85

[Article by I.I. Safronov and I.A. Leurda, Kishinev; UDC 621.789.2:534.8]

[Abstract] The authors of the study reported herein have analyzed the solution of a wave equation for the case of the vibrations of a waveguide wire during ultrasound treatment of metal melts. The theoretical analysis results are compared with the results of an experiment examining the effect of the properties of a tin melt on the resonance frequency of the wire's vibrations. A segment of steel wire 2 mm in diameter and 155 mm long was used for the experiments. A type UZG2-0.1 oscillator with continuous frequency regulation was used as the vibration source. A ChZ-36 frequency meter was used to measure the frequency of the vibrations, and a specially manufactured differential inductive amplitude sensor calculated by means of an optical microscope and with a measurement range of 0-50 μm was used to measure the amplitude and adjust the wire to resonance. The experiments were performed at different vibration amplitudes ranging from five to 20 μm, and the resonance frequency of an unloaded wire amounted to 22,330 Hz. After the wire was immersed a depth of three mm into the melt, the amplitude of the vibrations dropped to 30 percent of their initial value. The technique of changing the oscillator's frequency was used to restore the resonance mode in which the amplitude of the vibrations reached a level of 80 percent of their initial value. The decrease in the wire's resonance frequency turned out to depend on the amplitude of the vibrations. When the amplitude of the vibrations of the immersed wire reached 9 μm, the resonance frequency was about 490 Hz. At amplitudes above 9 μm, the drop in the wire's natural vibration frequency amounted to only 360 Hz. This finding was explained by the occurrence of cavitation in the melt at the specified amplitude. The appearance of cavitation bubbles in turn led to a decrease in melt density and hence the reactive component of the load's impedance. This in turn caused the detuning of the system. The experimentally detected change in detuning was, according to the expression derived by the authors, determined to correspond to about a 25 percent decrease in melt density. The results obtained led the authors to conclude that their proposed analysis technique is a simple method of determining the moment of onset of cavitation. Figures 2; references 4; Russian.

Properties and Use of Uranium-Fluorine Plasma. Part 2: Recovery of Uranium from UF₆ Without Reactants in High-Frequency Discharge Without Electrodes Discharge

927D0159E Moscow FIZIKA I KHIMIYA
OBRABOTKI MATERIALOV in Russian No 1,
Jan-Feb 91 (manuscript received 20 Mar 91) pp 61-67
[Article by Yu.N. Tumanov and K.V. Tsirelnikov,
Moscow; UDC 621.039.61:669.822]

[Abstract] An experimental study of U-F plasma was made for a practical purpose, to establish the feasibility of recovering uranium from UF₆ by atomization of that compound without use of reactants in an electric discharge and without use of electrodes and subsequent separation of the two elements. The apparatus for the experiment consisted of a radio-frequency oscillator and a discharge-reactor chamber, an inductor coil wound around that

chamber and coupling it to the oscillator, also a container with UF_6 condensate, in a thermostat, feeding that condensate to the discharge-reactor chamber through a heated tube with two valves and a flow meter, an argon tank feeding this gas to the discharge-reactor chamber as necessary through a tube with a valve, a container for UF_6 decomposition products underneath the discharge-reactor chamber, a quenching device inside this container for slowing down the recombination reaction and accelerating the condensation process, a filter for separating the UF_6 decomposition products and passing fluorine on to a converter with KI crystals where it is converted to iodine by way of the $2\text{KI (solid)} + \text{F}_2 \text{ (gas)} \rightarrow 2\text{KF (solid)} + \text{I}_2 \text{ (solid)}$ reaction, this converter in a thermostat being followed by a condenser in a thermostat, and the condenser being connected through a tube to a vacuum chamber. The discharge-reactor chamber was a water-cooled hollow copper cylinder with slots for dielectric inserts. The pressure inside this chamber was measured with an optical manometer. The quenching device was a cooled copper drum with a scraper, a set of stationary vibrating heat exchangers, and a nozzle for injection of an argon jet flooding the U-F plasma stream. Stable discharge at a frequency of 10 MHz was sustained under pressures not exceeding the 2000-2700 Pa range with an oscillator power of 15-20 kW, at a frequency of 17 MHz under pressures up to 4000 Pa with the same oscillator power, and at a frequency of 2450 MHz even under atmospheric pressure. Three methods of quenching a U-F plasma fast, at rates of 10^6 - 10^8 K/s, and in this way controlling the composition of UF_6 decomposition products are considered. The simplest method is mixing the content of the hot stream with a jet of cold gas or liquid. The second method is cooling the stream gas dynamically in a DeLaval nozzle, placement of a heat exchanger here being necessary in order to prevent reheating of the gas stream within the stagnation zone. The third method is cooling the stream in a tubular or finned recuperative heat exchanger. A temperature and pressure dependence of the quenching rate in each case is established on the basis of a quantitative analysis of respective chemical reactions and physical processes in accordance with the corresponding equations of thermodynamics and kinetics. Such an analysis indicates that estimates based on this experimental study are not very reliable, inasmuch as they have not yet been verified by a precise diagnostic study. Figures 3; tables 2; references 18.

Investigation of Mechanical Properties of NiAl-Based Materials Produced by Self-Propagating High-Temperature Synthesis Method

927D0163C Moscow ROSSIYSKAYA AKADEMIYA
NAUK: SERIYA METALLY in Russian No 2,
Mar-Apr 92 pp 128-134

[Article by A.G. Nikolayev, V.G. Koshelyayeva, V.N. Geminov, K.B. Povarova, Ye.A. Levashov, Yu.V. Bogatov, I.P. Borovinskaya, Moscow; UDC 536.421.5;536.46:621.762]

[Abstract] The urgent need for high-temperature and heat-resistant materials operating above Ti and Ni alloy working temperature ceiling and methods of making nickel

aluminide alloys are discussed; the possibility of using self-propagating high-temperature synthesis (SVS) for making NiAl-based materials; and an alloy of NiAl with Y_2O_3 is examined. Refractory thermodynamically stable yttrium oxide is selected as the hardening phase which is inert to the matrix and is resistant to oxidation. The effect of the self-propagating high-temperature synthesis conditions on the mechanical properties of the resulting specimens is also considered. Disc-shaped samples are synthesized from a mixture of powders mixed in a ball mill; composite Ni-Al particles are produced by two methods to increase the homogeneity of large products. The effect of the HV hardness on the self-propagating high-temperature synthesis process parameters and the temperature dependence of the limit of elasticity and modulus of elasticity calculated from the results of bending tests are plotted. The compacted dense samples produced by the self-propagating high-temperature synthesis method have satisfactory mechanical properties and demonstrate that the process is stable within a broad range of parameters. The mechanical properties of the SVS-NiAl samples are at a level of NiAl hardened with TiB_2 and HfC. Figures 3; references 8: 4 Russian, 4 Western.

Powder Titanium Oxidation During Heating in Air Medium

927D0164A Kiev POROSHKOVAYA
METALLURGIYA in Russian No 3(351),
Mar 92 pp 1-5

[Article by V.V. Tavgen, Ye.V. Shinkareva, Ye.V. Karpinchik, Yu.G. Zonov, General and Inorganic Chemistry Institute at the Belarussian Academy of Sciences, Minsk; UDC 669.295]

[Abstract] The dependence of the stability of properties and operating reliability of composite conducting coats on the oxidation degree of titanium added to composites with inorganic binders as a conducting filler for making resistive coats is discussed, and the processes of oxidation in the air of finely disperse ($<40 \mu\text{m}$) PTOM titanium (TU 14-1-3086-80) produced by hydride calcium reduction are investigated by differential thermal (DTA) and X-ray phase analyses and electron microscopy within a 20-960°C temperature range. A complex thermal analysis is performed in a MOM derivatograph at a 5°/min temperature rise rate while the X-ray diffraction analysis is performed in a DRON-3 in CuK radiation on a Ni filter with a GPVT-1500 high-temperature recording attachment. The complex thermal analysis made it possible to identify four powder titanium oxidation stages in the air. The findings indicate that slow oxidation of finely disperse titanium commences at 280°C and rises sharply at 600-620°C while the resulting dense oxide film plays a passivating role by limiting oxygen access to the Ti surface. At the concluding stage of oxidation at 700-720°C, the oxide film acquires a coarse crystalline structure and porous texture. As the temperature increases further, the processes terminate in total titanium oxidation to TiO_2 . Figures 5; references 7: 6 Russian, 1 Western.

Effect of Structure on Deformation of Metal Fabric for Composite Reinforcement

927D0164C Kiev POROSHKOVAYA
METALLURGIYA in Russian No 3 (351),
Mar 92 pp 20-26

[Article by L.R. Vishnyakov, L.I. Feodosyeva, S.N. Yakimenko, Institute of Materials Science Problems at the Ukrainian Academy of Sciences, Kiev; UDC 660.22-419]

[Abstract] Reinforcement of the metallic composite (KM) matrix used as a powder or thin foil with a metal mesh or knitted fabric for ensuring the necessary anisotropy of properties corresponding to the material's operating conditions and the structural advantages of such reinforcements are discussed and an attempt is made to develop a computational model on the basis of a loop representative element using the example of "lastic" and "fang" type knitted fabric structures. The elongation of net sheets made from bundles of two and five filaments, depending on the tensile load, net sheet transverse deformation and elasticity moduli and the loading and deformation diagrams of the fang representative element are plotted. The procedure for calculating the reinforcement deformation and moduli of elasticity makes it possible to design knitted metal fabric reinforcement nets for composite materials with given mechanical properties for specific operating conditions. An experimental check of the analytical values demonstrates the consistency of the model. Figures 6; tables 1; references 7.

Hot Extrusion of Aluminum Alloy Granules in Two-High Rolling Mill

927D0164D Kiev POROSHKOVAYA
METALLURGIYA in Russian No 3 (351),
Mar 92 pp 26-28

[Article by V.N. Kornilov, N.V. Shepelskiy, Krasnoyarsk Nonferrous Metals Institute; UDC 621.777]

[Abstract] The use of aluminum alloy pelletizing with subsequent product and semifinished item fabrication by plastic metal working which improves the mechanical properties of alloys and makes it possible to utilize secondary aluminum raw materials as well as open up the possibility of producing new conducting and high-temperature materials and the lack of specialized machines for processing the loose metallic body into products which constraints further development of the granule technology are discussed. A device capable of forming aluminum alloy granules into products in which continuous extrusion from a closed pass is performed by active friction forces is proposed; two rolls—with a groove and a ridge—form the pass with a die block on the outlet. A schematic diagram of the new device is cited and a formula is derived for calculating the extrusion pressure developed by active friction forces on the basis of the thin sections method. The method of continuous rolling and extrusion of aluminum alloy granules from the closed pass under the effect of active friction forces makes it possible to produce items with a higher level of mechanical properties compared to extrusion in vertical hydraulic presses. Figures 3; references 3.

Porous Copper-Based Fibrous Powder Materials

927D0164G Kiev POROSHKOVAYA
METALLURGIYA in Russian No 3 (351),
Mar 92 pp 56-60

[Article by M.V. Tumilovich, A.G. Kostornov, A.N. Leonov, V.K. Sheleg, V.M. Kaptsevich, Belarussian Republican Scientific Production Association of Powder Metallurgy, Minsk, and Institute of Materials Science Problems at the Ukrainian Academy of Sciences, Kiev; UDC 621.762.5]

[Abstract] The shortcomings and advantages of porous permeable materials and particularly porous powder materials (PPM) and porous fibrous materials (PVM) are discussed, and an attempt to develop porous permeable materials from a mixture of powder and fibers which have the positive features of porous powder materials and porous fibrous materials, i.e., combine their relatively fine filtering properties with good permeability and plasticity, is reported. The properties of a uniform composition consisting of an electrolytic PMS copper powder and a fiber produced by cutting to size of M1 copper wire are investigated and several methods of mixing the powder with fibers are outlined. The characteristics of the original components are summarized, and the technological, hydrodynamic, and physical-mechanical properties of the sintered products are examined. The effect of the fiber concentration and compaction pressure on the material porosity, efficiency criterion, infiltration rate, maximum and mean pore dimensions, permeability coefficient, ultimate strength, elongation, volume shrinkage during sintering, and electric conductivity is plotted, and the topogram of a composite with 20 percent fiber compacted at a 28 MPa pressure is cited. The dependence of the Balshin formula exponent on the fiber concentration in the material is examined. It is shown that the permeability and plasticity of a composite with 80 percent fiber compacted at 5 MPa are 15 and 1.4 times greater than those of a fiber material while the pore size is 1.3 times smaller. The wide range of variation in properties and the ambiguous correlation between them create the conditions for designing materials with a specified range of physical, mechanical, and operating properties and makes them promising for practical uses. Figures 3; tables 1; references 4.

Structure Formation and Electric Conductivity in Thick Disperse Ni_3B Powder-Based Films

927D0164H Kiev POROSHKOVAYA
METALLURGIYA in Russian No 3 (351),
Mar 92 pp 71-75

[Article by Yu.K. Kulba, B.M. Rud, I.M. Vinitskiy, Institute of Materials Science Problems at the Ukrainian Academy of Sciences, Kiev; UDC 546.43'27+546.654'27]

[Abstract] The high cost of precious metals used as the functional base in thick film technology prompted a search for their substitutes—refractory borides that form a low-melting boric anhydride at the early processing stages that envelops the functional phase particles and additionally protects them from oxidation. The phase and structural transformations occurring in thick film conductors on the

basis of disperse Ni_3B powders during their heat treatment in the air and the effect of these processes on the development of the film's electrophysical properties are investigated. Thermogravimetric curves of the Ni_3B powder under heating in the air, X-ray diffraction spectra of the original powder and powder annealed in the air at various temperatures, the temperature dependence of magnetic susceptibility of the original and air-annealed powder, and the behavior of electric resistivity of a Ni_3B -based film during heat treatment are plotted. The electric properties of thick film Ni_3B -based conductors are summarized. An analysis demonstrates that boride films oxidize in the air during heat treatment forming metallic nickel and boric anhydride which plays the role of a vitreous binder and compacts the conducting particles thus ensuring their adhesion to the substrate. To produce highly conducting films, the heat treatment conditions and dispersivity of the original powder must be matched so as to ensure that the boric anhydride volume is sufficient to consolidate the film yet insufficient to form insulating layers between the particles. Conducting phase particles form mutual contacts with a tunnel electric conductivity mechanism. Figures 5; tables 1; references 5.

Effect of Electrode Composite Materials' Composition and Structure on Their Erosion Character and Discharge Dynamics in Railtron

927D0164I Kiev POROSHKOVAYA METALLURGIYA in Russian No 3 (351), Mar 92 pp 75-80

[Article by V.P. Zinovyeva, A.D. Lebedev, R.B. Luban, K.V. Malevinskiy, Thermal Physics Institute at the Siberian Branch of Russia's Academy of Sciences, Novosibirsk, and Institute of Materials Science Problems at the Ukrainian Academy of Sciences, Kiev; UDC 669.018.95;537.523]

[Abstract] The processes of current and mass transport on the plasma boundary with the electrode in electrodynamic accelerators and railtrons and their effect on the electrode erosion are discussed, and it is noted that composite materials produced by powder metallurgy methods are the most promising for use as electrodes in the railtron channel since they meet the requirements imposed on their thermal and electric properties. The presence of special additives in these electrodes and their structural modifications may change both the discharge structure and the dynamics of its movement in the electrode. Electrodes made from Cu with inclusions of the emission active phase (EAF), Cu disperse-hardened by Al_2O_3 particles, and copper coated with a refractory ultradisperse powder (UDP) are tested; the electrode surface is analyzed under a MIM-7 microscope. The dependence of the plasmoid leading and trailing edge coordinate on the time of its movement in an electrode from bronze with an ultradisperse powder, bronze with cadmium, and other materials, the time behavior of the plasmoid leading edge velocity in an electrode from bronze with an ultradisperse powder, bronze with cadmium, and other materials, and the dependence of the plasmoid leading and trailing edge velocity on their coordinate during movement in electrode from composite materials (Cu-LaB_6 and Mo-Cu-LaB_6) are plotted. Thus, inclusions

of the emission active phase substantially affect the character of railtron electrode erosion and the current and heat transfer in the discharge and increase the erosion resistance and the degree of discharge propagation on the electrode's working surface. The latter is largely due to an increase in the dispersivity of all composite constituents and their uniform distribution in the electrode material as well as the presence of a refractory core. Mo-Cu-LaB_6 electrodes are recommended for use in railtrons. Figures 4; tables 2; references 14: 13 Russian, 1 Western.

Experience of Making Hard Alloy Cutting Tools by Self-Propagating High-Temperature Synthesis Method

927D0164K Kiev POROSHKOVAYA METALLURGIYA in Russian No 3 (351), Mar 92 pp 92-97

[Article by S.M. Vaytsekhovich, A.A. Mishulin, Scientific Production Association of the Central Scientific Research Institute of Machine Building Technology, Moscow; UDC 621.762.4;546.07;536.46]

[Abstract] The unique properties of hard alloys—wear-resistant metallic materials with a high natural hardness in equilibrium conditions which retain it at elevated temperatures—and a search for substitutes for scarce tungsten used as their basis are discussed, and attention is focused on the method of self-propagating high-temperature synthesis (SVS). The experience of making cutting tips from synthetic hard tool materials (STIM) whose physicomechanical properties are at the level of domestic VK, TK, TTK, and TN hard alloys is summarized. It is shown that the most efficient and economical method involves adding to the production process several molding devices according to the operational stage principle. The methods developed at the TsNIITMASH for making an isotropic billet which include cold molding of the initial agents plasticized with mixtures of inorganic solvents with synthetic polymers are outlined and a technology which involves mixing the original components, molding them into isotropic briquettes, thermal synthesis, compacting the synthesis products into billets with a given density, cutting the synthetic billet into tips, tumbling and heat treating them, and grinding the tips to size is summarized. The new process also makes it possible to make large products on a commercial scale whose dimensions exceed the possible billet dimensions produced by powder metallurgy by several times. Figures 4; references 12.

Dynamics of Multistage Purification by Zone Recrystallization

927D0165A Moscow VYSOKOCHISTYYE VESHCHESTVA in Russian No 2, Mar-Apr 92 pp 7-15

[Article by G.G. Devyatykh, V.A. Dozorov, Yu.P. Kirillov, M.F. Churbanov, High-Purity Substance Chemistry Institute at Russia's Academy of Sciences, Nizhny Novgorod, and Scientific Research Institute of Applied Mathematics and Cybernetics at the Nizhny Novgorod State University; UDC 66.011.01;669.049.44]

[Abstract] The advantages and limitations of zone recrystallization for multiple stage purification processes and the task of simulating the process and especially the late passes leading to a steady-state purification limit are discussed; the features of the multistage purification process dynamics and statics are analyzed in a typical case of multistage recrystallization at a constant melt zone length. To this end, the steady-state impurity distribution along the ingot length is formulated, and the state space of the system is introduced in the form of mean concentrations from the ingot start to its current cross section; the process dynamics are considered in this space at various molten zone lengths. The material balance equations and the boundary value and initial conditions—a cellular model of the process—are derived in a nondimensional form. A computational experiment is conducted to determine the evolution of the impurity amount in the ingot during the

process and the dependence of the purification index on the number of model zones, the dependence of the impurity concentration decrease rate in the ingot on the number of passes, the dependence of the normalized purification factor on the number of passes, the dependence of the extended purification front on the number of zones, and the dependence of the steady-state level relaxation time on the product yield fraction are plotted. The effect of the product yield fraction on the front duration and dynamic curves of the purification factor are analyzed. The character of steady-state relaxation rate curves differs substantially at early and late passes. The computational experiment makes it possible to determine the static and dynamic characteristics of the process under specific high-degree purification conditions when the number of passes increases by tens and hundreds of times. Figures 7; references 10: 6 Russian, 4 Western.

Calculated and Experimental Estimates of the Parameters of the Activation of Alloys Based on Aluminum and Vanadium by the Neutrons of Fission and Synthesis Reactors

927D0158G Moscow ROSSIYSKAYA AKADEMIYA
NAUK: SERIYA METALLY in Russian No 1,
Jan-Feb 92 (manuscript received 14 Jan 91) pp 141-145

[Article by L.I. Ivanov, V.V. Ivanov, V.P. Kolotov, Yu.M. Platov, and V.I. Tovtin, Moscow; UDC 669.715+669.292.5:621.039.548]

[Abstract] The authors of the study reported herein made calculated and experimental estimates of the activation parameters of aluminum- and vanadium-based alloys by the neutrons of fission and synthesis reactors. Specifically, they made numerical estimates of the level and kinetics of the decay of induced radioactivity in hypothetically pure aluminum, titanium, vanadium, and a number of alloys based on them for fission and synthesis reactor spectra all the way up to neutron fluences of $10^{27}/\text{m}^2$. The studies performed established that vanadium-titanium alloys may be considered promising radiation-resistant materials for use in the primary wall of thermonuclear d-T synthesis reactors. The studies performed indicated that the said alloys meet ecological requirements regarding induced radioactivity to a much greater extent than do other metallic construction materials. Aluminum-based alloys, particularly alloys based on the system aluminum-magnesium-scandium, were found to be promising as highly radiation-resistant materials for use in the components and structures of fission reactors. The same conclusion was reached for alloys of the vanadium-titanium system. The studies further indicated that in d-T synthesis reactors, alloys based on aluminum, vanadium, and titanium may be used as radiation materials outside primary reactor loop or else for use in softened neutron spectra. The technique of degassing the radionuclides ^{39}Ar and ^{36}Cl in vanadium and titanium was shown to be a promising process for use in burying radioactive wastes made of these materials. The technique of γ -spectroscopy was used to investigate the radionuclide profile and estimate the radioactivity of aluminum, vanadium, and their alloys when irradiated by a neutron fluence of $10^{24}/\text{m}^2$ in an SM-2 reactor. Specifically, specimens of 99.999 percent pure aluminum and alloys consisting of 1) Al + 2 percent Mg + 0.4 percent Sc, 2) Al + 2 percent Mg + 0.2 percent Sc, and 3) V + 21.5 atomic percent Ti were irradiated in an CM-2 reactor with a neutron fluence of $5 \times 10^{24}/\text{m}^2$ and held for five to six years before the analysis. The irradiated aluminum and aluminum alloys were found to contain long-lived radionuclides (^{137}Cs and ^{60}Co) that significantly increased the length of time required for the materials to reach a biologically safe level after irradiation in a fission reactor. An analogous pattern was found for the fission spectrum in the case of alloy 3. The long-lived radionuclides ^{60}Co , ^{182}Ta , and ^{94}Nb found to have formed on W, Mo, Ni, Ta, and Nb impurities significantly modified the

activation parameters and kinetics of the subsequent decay of the alloy's induced radioactivity. While a hypothetically pure alloy of V plus 21 atomic percent Ti should reach a biologically safe level in fewer than 30 years, the decay of the radionuclide ^{60}Co increases the time required to reach a safe level to 35 years. The presence of ^{94}Nb increases the said period to 10^5 years. The studies performed thus established that the problem of creating materials for use in nuclear power engineering that do not become highly activated by the neutrons of fission and synthesis reactors is largely a problem of creating pure bases and components of alloys that are free of impurities resulting in the formation of long-lived radionuclides. Figures 2; tables 2; references 8: 6 Russian, 2 Western.

Thermal Impact Loading of Metal by Pulsed Proton Beam

927D0159C Moscow FIZIKA I KHIMIYA
OBRABOTKI MATERIALOV in Russian No 1,
Jan-Feb 92 (manuscript received 5 Mar 91) pp 29-33

[Article by V.I. Boyko, I.V. Shamanin, and K.V. Yushitsin, Tomsk; UDC 539.4.015.5]

[Abstract] Action of a pulsed ion (proton) beam on a metal target which does not melt that target but results in purely thermoelastic generation of an acoustic stress pulse in it is considered, propagation of such a pulse through such a target and its subsequent reflection by the back surface being analyzed mathematically on the basis of two equations: 1) classical equation of transient one-dimensional heat conduction, 2) classical wave equation for propagation of mechanical strain during linear thermal expansion under a temperature gradient. The waveform and time characteristics of both the beam-accelerating voltage pulse and the beam-current pulse do, for this analysis, simulate those in an experiment with a magnetically shielded diode (V.M. Bystritskiy and V.I. Boyko; FIZIKA PLAZMY Vol 15 No 11, 1989). The metal is assumed to have a high proportional limit and to fracture immediately after a slight plastic deformation not larger than its elastic deformation. The problem has been thus reduced to one of mechanical thermoelasticity. Both surfaces of the metal plate are assumed to be perfectly soft so that they totally reflect incident acoustic pulses and to be radiating heat into vacuum. This system of two equations is solved by numerical integration using a homogeneous implicit difference scheme and the elimination method. The results of calculations for an aluminum plate indicate that as the incident ion current pulse at the front surface ends, there begins to form a bipolar pulse of thermal stress in the plate. This pulse then propagates at some velocity toward the back surface, its amplitude remaining constant until that surface is reached and then increasing upon reflection and attendant inversion of the pulse by the back surface. All this takes place during much more prolonged thermoelastic stressing of the target within the region adjacent to its bombarded surface. Figures 3; references 7.

Effect of Hardening Conditions on Mechanical Properties and Residual Stresses in High-Temperature EP962 Nickel Alloys

927D0161C Moscow METALLOVEDENIYE I
TERMICHESKAYA OBRABOTKA METALLOV
in Russian No 1, Jan 92 pp 10-13

[Article by V.I. Yermenko, N.N. Korneyeva, N.N. Zhuravlev, A.V. Kashcheyeva, V.D. Piskarev, L.P. Dashkevich, All-Union Institute of Light Alloys and Stupino Integrated Iron and Steel Works; UDC 669.14.018.44:621.785.6:620.172]

[Abstract] Deformed billets of the complex-alloyed EP962P nickel alloy containing more than 45 percent of the hardening γ' -phase and γ -solid solution with a high supersaturation degree produced by granule metallurgy and cast alloy EP962ID are examined after heat treatment; the billets are hardened in a steel crucible and their residual stress is measured in three zones in the axial and circumferential direction by the method of total prism release, using strain gauges. The billet cooling curves in oil and carnallite and residual volumetric stresses in billets after various types of treatment are plotted. An analysis of the effect of various quenching media and cooling rates on the level of residual stresses and mechanical properties of EP962 nickel alloy made it possible to recommend the following optimal quenching conditions: using alkali and salt melts as the quenching media at a starting quench temperature of 600°C and a cooling rate of 100-60°C/min. It is noted that after quenching in melts, the values of the rupture strength is somewhat lower than after oil quenching while after quenching in carnallite at 500°C, the strength properties are higher than after oil quenching. The level of residual stress after salt melt quenching is lower than after oil quenching by approximately twofold. It is stressed that the optimum quenching temperature, medium, and cooling rate ensure the γ' -phase precipitation with the necessary degree of dispersion. Figures 5; tables 2.

Effect of Straining Conditions in ($\alpha+\beta$)-Area on Structure and Properties of Titanium Pseudo- α -Alloy

927D0161J Moscow METALLOVEDENIYE I
TERMICHESKAYA OBRABOTKA METALLOV
in Russian No 1, Jan 92 pp 35-39

[Article by I.N. Razuvayeva, V.N. Kopylov, N.M. Dobrodeyeva, G.V. Medvedeva, Yu.D. Khesin; UDC 621.771:669.295.5:620.17]

[Abstract] The behavior of the structure and texture of an experimental titanium pseudo- α -alloy with a polymorphous transformation temperature of 1,040°C as a function of rolling temperature and straining pattern is examined in the ($\alpha+\beta$) area. To this end, 100 mm thick slabs are rolled first to a 50 mm thickness, then exposed for 30 min to the initial heating temperature, then exposed for two hours to a temperature of 950, 970, 1,000, and 1,020°C,

then rolled again to a 30 mm thickness. Mechanical and low cycle fatigue tests in a corrosive medium are performed and the alloy texture is examined by the inverse pole figure method (OPF). X-ray studies are carried out in DRON-UM and DRON-2.0 diffractometers in CuK radiation. The recrystallization process is analyzed by reverse filming by a KROS camera. The findings indicate that straining of the pseudo- α -alloy of titanium in the upper part of the ($\alpha+\beta$) area, i.e., from the melting point to a temperature 50°C below the polymorphous transformation point, which is accompanied by dynamic recrystallization leads to the development of a multicomponent texture regardless of the straining pattern. The resulting structure consists of recrystallized β -grains with a lamellar intragranular structure and individual round α -grains with serrated boundaries; this structure ensures quasiisotropic properties in the rolled sheet plane and high isotropic values of stress corrosion cracking. In the lower part of the ($\alpha+\beta$) area straining which is not accompanied by dynamic recrystallization leads to the development of either a predominantly prismatic structure or a deflected basis-type texture, depending on the straining pattern. Figures 3; tables 1; references 5: 3 Russian, 2 Western.

Effect of Aging on Structure and Elastic Properties of Hardened ($\alpha+\beta$) Titanium Alloys

927D0161K Moscow METALLOVEDENIYE I
TERMICHESKAYA OBRABOTKA METALLOV
in Russian No 1, Jan 92 pp 39-42

[Article by T.A. Panayoti, A.S. Gorbova (deceased), G.F. Taran, T.D. Kiseleva; UDC 620.17:620.18:669.295.5]

[Abstract] The unique properties of titanium ($\alpha+\beta$) alloys which combine excellent corrosion resistance, low density, high strength, a low modulus of elasticity, and sufficient ductility and are nonmagnetic are discussed, and the effect of the aging temperature and duration on the structure, phase composition, and properties of the VT3-1, VT9, and VT22 high-alloy ($\alpha+\beta$) titanium alloys is studied. The chemical composition of the alloys is summarized. Hot rolled alloy samples are water quenched at 830, 930, and 730°C and aged at temperatures within a 400-600°C range with exposures varying between one hour and ten hours. The structure of the aged alloy is examined metallographically and by electron microscopy and X-ray structural analysis with the help of a DRON-1 diffractometer in CoK radiation. The decay product morphology is generally determined from the aging duration and temperature. Both stable α - and β -phases and metastable α'' - and β'' -phases are found in the alloys. The effect of temperature and aging duration on the resistivity and limit of elasticity of alloys hardened at 830, 930, and 730°C is plotted. An analysis of the findings shows that the resistance of the VT3-1, VT9, and VT22 alloys to small plastic strain increases by twofold due to hardening heat treatment and aging at 500°C for 8 h. The alloys thus treated may be used as corrosion-resistant low-density spring materials. Figures 3; tables 6; references 4.

Improving Properties of Large Semifinished Items From VT23 Alloy by Thermal Cycling

927D0161L Moscow METALLOVEDENIYE I
TERMICHESKAYA OBRABOTKA METALLOV
in Russian No 1, Jan 92 pp 43-44

[Article by V.S. Lyasotskaya, A.I. Khorev, K.N. Sergeyev, S.I. Knyazeva, L.I. Gorbunova; UDC 621.785.789:669.295.5]

[Abstract] The nonuniform structure and properties of semifinished items from titanium alloys prompted a study of the effect of thermal cycling (TTsO) on the structure and properties of large semifinished items from the VT23 alloy. To this end, 80 mm thick slabs are tested in two states: the initial state with heterogranular structure after hot rolling and standard annealing at an 800°C temperature and the superheated state with a large grain structure after annealing at 1,000°C for two hours and air cooling. The sample microstructure is examined and the results of ductility, toughness, and tension tests are summarized. The structure is analyzed using a Neophot-30 metallographic microscope and a DRON-UM X-ray diffractometer. Test data and microstructural analyses demonstrate that the use of thermal cycling in the $\alpha+\beta$ area for large slabs in the initial hot rolled state makes it possible to increase its ductility and toughness while thermal cycling of the VT23 alloy in the superheated state in the same $\alpha+\beta$ area worsens its ductility. It is suggested that VT23 alloys with a superheated β -transformed structure be subjected to thermal cycling with a β -transition in order to spheroidize the α -phase and

improve its ductility and toughness; the evenly precipitated globular α -phase ensures a 1,190 N/mm² strength. Figures 1; tables 1; references 3.

On Possibility of Removing Fluorine From Silicon Nitride Powder Surface by Chemical Reagents

927D0164B Kiev POROSHKOVAYA METALLURGIYA
in Russian No 3 (351), Mar 92 pp 5-7

[Article by G.N. Komratov, Yu.M. Shulga, Branch of Chemical Physics Institute at Russia's Academy of Sciences, Chernogolovka; UDC 621.762]

[Abstract] The effect of technological impurities on the sintering of powders and operating properties of products made by powder metallurgy methods from silicon nitride powders is discussed, and the distribution and state of fluorine ions—an impurity element in N-1 silicon nitride powder (produced by Stark)—is investigated by X-ray photoelectron spectroscopy (RFS). The structure of the 4 nm thick near-surface solid layer is examined. In order to determine the total fluorine concentration in the powder, interfering metals are first removed in the form of hydroxides; then a 45 percent aqueous HF solution is used to pickle the silicon nitride surface. The element concentration in the bulk and on the surface of silicon nitride samples is summarized. The results show that HF pickling is efficient in removing surface fluorine with a weight loss not exceeding 10 percent. The principal proportion of the fluorine impurity is concentrated in the near-surface particle layer in the form of SiF and/or SiF₂ fragments and can be thus easily removed by HF. Tables 1; references 4: 1 Russian, 3 Western.

Selected Features of the Interconnection of the Genesis, Chemicomineralogic Makeup, and Reducibility of Manganese Ore Materials From Different Deposits. Part 4: Selected Characteristic Features of the Mechanism of the Carbon Reduction of Manganese Ore Materials

927D0158A Moscow ROSSIYSKAYA AKADEMIYA
NAUK: SERIYA METALLY in Russian No 1,
Jan-Feb 92 (manuscript received 12 Apr 90) pp 5-12

[Article by S.G. Grishchenko, T.F. Raychenko, and N.M. Moskaleva, Zaporozhye; UDC 669.74:621.78]

[Abstract] The authors of the study reported herein conducted a series of experiments demonstrating the possibility of partial solid-phase metallization of manganese that entails the appearance of a metal phase at low and moderate temperatures. This phase is the product of the disproportionation of lower suboxide metastable compounds formed as a result of dehydration of starting hydrate, hydroxide, and hydrocarbonate compounds. Specifically, to confirm their hypothesis of the existence of manganese oxides that have an oxygen deficit and that remain stable at high temperatures, the researchers mixed powdered high-purity manganese oxide with a powder of metallic electrolytic manganese. Pyrolusite-type oxide ore from the Nikopol area, gas carbon, and graphite were used in the experiments. The fraction of reducing agent in the initial mixture was varied from 1 to 30 percent by mass. The initial mixture was pelletized into granules that were then annealed in a reducing atmosphere at a temperature of 1,200°C for half an hour. The pellets were annealed in a weakly reductive atmosphere at temperatures ranging from 600 to 1,500°C. Samples were taken at 100°C intervals. Crystalline optic studies and X-ray spectral microanalysis were performed on the samples. An examination of the microstructure of the cooled reaction products showed that a nonstoichiometric phase with an

oxygen deficit does indeed form when the two forms of manganese react with one another. The studies further demonstrated that timely evacuation of the gaseous dehydration-decarbonization products (namely, H_2O and CO_2) oxidizing the intermediate phases with an oxygen deficit to a stable state and thereby suppressing the disproportionation process is a necessary condition of the process. The initial generation of a metallic phase was established to occur at a temperature of 800 to 850°C. The phase formed was in the form of disperse metal beads mixed with an "unstructured" oxide phase. The microstructure of these products was similar to an emulsion characteristic of the decomposition of solid solutions. The studies confirmed the important role of a solid carbon reducing agent that is broken into pieces along with the manganese ore in changing the temperature interval in which reduction processes occur, as well as the degree to which the said processes occur. Increasing the heat treatment temperature to 1,000°C in the presence of a reducing agent was found to intensify the formation of metastable oxides with an oxygen deficit. A second generation of metal was found to occur in the products of annealing with a reducing agent in the temperature interval from 1,100 to 1,200°C. This metal was in the form of larger metal beads. A third generation of metal was ascribed to the temperature interval from 1,250 to 1,350°C. The metal beads formed were determined to be manganese sulfide and silicon dioxide neoplasms, thus confirming the complex makeup of the metal-forming subcompounds existing close to lower oxysulfides. As the temperature was increased to 1,400-1,500°C with a reducing agent present, the specimens began to break up and transform into powder. The appearance of a fourth generation of metal under these conditions was linked to the participation of complex oxycarbide compounds in the reaction (as confirmed by the stable disproportionation products detected). Figures 5; references 10: Russian.

Reagent-Free Fluorine-Containing Waste Water Treatment

927D0153C Moscow STEKLO I KERAMIKA
in Russian No 1, Jan 92 pp 6-8

[Article by B.L. Prisyazhnyuk, Kishinev State Teachers College; UDC 666.21.004.9:628.3]

[Abstract] The difficulties of waste water treatment with the help of reagents, especially at low fluorine concentrations, are outlined, and a new electrolytic reagent-free method of fluorine waste water treatment which is based on electrolytic dissolution of aluminum electrodes during the passage of electric current through an aqueous solution is described. A schematic diagram of the electrolytic unit is shown, and the degree of fluorine removal from waste water and final water pH as a function of the electric

current outlays for defluorination, the dependence of the defluorination degree on the cathode current density and process duration, and the effect of waste water pH on the defluorination degree are summarized. The sodium, potassium, calcium, magnesium, chlorine, and iron ion and sulfate, nitrate, hydrocarbonate, and fluorine concentration in the solution before and after treatment are cited. The F^- concentration is reduced from 2.6-3.4 to 1.3-1.6 mg/l. The electrolytic unit is tested at the Tiraspol Glass Container Plant at an initial solution pH = 6.9-7.2; after the treatment, the index is increased to 7.0-7.4 and the temperature varies within 16-18 to 20-21°C, respectively. The reagent-free method makes it possible to remove residual fluorine ions and lower its concentration to the maximum permissible level. N.T. Okopnaya helped with chemical analyses. Figures 1; tables 4; references 4.

NTIS
ATTN PROCESS 103
5285 PORT ROYAL RD
SPRINGFIELD VA

2

22161

This is a U.S. Government publication. Its contents in no way represent the policies, views, or attitudes of the U.S. Government. Users of this publication may cite FBIS or JPRS provided they do so in a manner clearly identifying them as the secondary source.

Foreign Broadcast Information Service (FBIS) and Joint Publications Research Service (JPRS) publications contain political, military, economic, environmental, and sociological news, commentary, and other information, as well as scientific and technical data and reports. All information has been obtained from foreign radio and television broadcasts, news agency transmissions, newspapers, books, and periodicals. Items generally are processed from the first or best available sources. It should not be inferred that they have been disseminated only in the medium, in the language, or to the area indicated. Items from foreign language sources are translated; those from English-language sources are transcribed. Except for excluding certain diacritics, FBIS renders personal names and place-names in accordance with the romanization systems approved for U.S. Government publications by the U.S. Board of Geographic Names.

Headlines, editorial reports, and material enclosed in brackets [] are supplied by FBIS/JPRS. Processing indicators such as [Text] or [Excerpts] in the first line of each item indicate how the information was processed from the original. Unfamiliar names rendered phonetically are enclosed in parentheses. Words or names preceded by a question mark and enclosed in parentheses were not clear from the original source but have been supplied as appropriate to the context. Other unattributed parenthetical notes within the body of an item originate with the source. Times within items are as given by the source. Passages in boldface or italics are as published.

SUBSCRIPTION/PROCUREMENT INFORMATION

The FBIS DAILY REPORT contains current news and information and is published Monday through Friday in eight volumes: China, East Europe, Central Eurasia, East Asia, Near East & South Asia, Sub-Saharan Africa, Latin America, and West Europe. Supplements to the DAILY REPORTs may also be available periodically and will be distributed to regular DAILY REPORT subscribers. JPRS publications, which include approximately 50 regional, worldwide, and topical reports, generally contain less time-sensitive information and are published periodically.

Current DAILY REPORTs and JPRS publications are listed in *Government Reports Announcements* issued semimonthly by the National Technical Information Service (NTIS), 5285 Port Royal Road, Springfield, Virginia 22161 and the *Monthly Catalog of U.S. Government Publications* issued by the Superintendent of Documents, U.S. Government Printing Office, Washington, D.C. 20402.

The public may subscribe to either hardcover or microfiche versions of the DAILY REPORTs and JPRS publications through NTIS at the above address or by calling (703) 487-4630. Subscription rates will be

provided by NTIS upon request. Subscriptions are available outside the United States from NTIS or appointed foreign dealers. New subscribers should expect a 30-day delay in receipt of the first issue.

U.S. Government offices may obtain subscriptions to the DAILY REPORTs or JPRS publications (hardcover or microfiche) at no charge through their sponsoring organizations. For additional information or assistance, call FBIS, (202) 338-6735, or write to P.O. Box 2604, Washington, D.C. 20013. Department of Defense consumers are required to submit requests through appropriate command validation channels to DIA, RTS-2C, Washington, D.C. 20301. (Telephone: (202) 373-3771, Autovon: 243-3771.)

Back issues or single copies of the DAILY REPORTs and JPRS publications are not available. Both the DAILY REPORTs and the JPRS publications are on file for public reference at the Library of Congress and at many Federal Depository Libraries. Reference copies may also be seen at many public and university libraries throughout the United States.